J. Fluid Mech. (1982), *vol.* 123, *pp.* 1–29
Printed in Great Britain

Experiments on the role of amplitude and phase modulations during transition to turbulence

By R. W. MIKSAD, F. L. JONES,
Water Resources Group,
The University of Texas at Austin,
Austin, Texas 78712

E. J. POWERS, Y. C. KIM AND L. KHADRA
Electronics Research Center,
The University of Texas at Austin,
Austin, Texas 78712

(Received 17 December 1980 and in revised form 22 February 1982)

The transition of a laminar two-dimensional wake is studied experimentally to establish the role of amplitude and phase modulations in the spectral-broadening and energy-redistribution process. Multiple instability modes f_0 and f_1 are triggered by acoustic excitation. The spectrum of the fluctuating velocity field formed by the growing and interacting instabilities shows the development of a complicated sideband structure reminiscent of amplitude- and phase-modulated waves. Digital complex demodulation techniques are used to obtain quantitative measurements of local instantaneous amplitude and phase modulations. Measurements of the modulation time traces, their modulation indices, the lag between phase and amplitude modulations, and the power spectra of the modulations are presented. Our results show that both phase and amplitude modulation play a role in the transition process. The dominant modulation frequency of both amplitude and phase is that of the difference mode $f_\nu = f_1 - f_0$ produced by the interaction of the two excited instabilities. Phase modulation becomes progressively more important as transition proceeds downstream, and seems to play the dominant role in the spectral-broadening and energy-redistribution process. Measurements of the bicoherency spectrum indicate that sideband structures, and accompanying modulations, are produced by nonlinear interactions between the low-frequency difference mode and higher-frequency instability modes. Some limited measurements indicate that finite-amplitude induced nonlinear dispersion effects $\omega(k, a^2)$ may provide a physical mechanism by which amplitude modulations generated by nonlinear interactions can induce simultaneous phase modulations.

1. Introduction

The experiments of Sato (1970), Sato & Saito (1975) and Motohashi (1979) indicate that nonlinear interactions during the laminar–turbulent transition of a two-dimensional wake produce a distinct change in the character of fluctuations observed in the flow. Initially, background noise or externally introduced controlled disturbances trigger instability of a limited band of exponentially growing waves. As these instabilities grow, nonlinear interactions generate new fluctuations at lower and higher

frequencies through difference and sum interactions of the dominant instability modes. The results of Motohashi (1979) indicate that nonlinear interactions between waves at the dominant instability frequencies and lower-frequency fluctuations can lead to the generation of new fluctuations at multiple sideband frequencies. Sato (1970) and Sato & Saito (1975) suggest that nonlinear interactions can lead to amplitude modulations of the instability waves. In natural transition, the modulation may have a random character. In controlled transition, discrete low-frequency waves modulate the instability modes. In both situations, modulations of the fluctuating velocity field seem to play an important role in the transition process.

Gertsenshtein, Sukhorukov & Shkadov (1977), in a theoretical study of nonlinear interactions in a two-dimensional wake, concluded that low-frequency modulations of instability fluctuations do play an important role in spectral energy redistribution and randomization, and that phase (or frequency) modulation may be a significant feature of this process. Sato & Saito (1975) suggest that demodulation of amplitude-modulated waves may play a role in spectral energy redistribution; the demodulation arises from the nonlinearity of wave–wave interactions. Theoretical studies by Kim, Khadra & Powers (1980) and Bakai (1970) on general three-wave interactions have demonstrated that nonlinear interactions between instability modes and lower-frequency waves can generate an instability mode with low-frequency modulations in phase, $p(\mathbf{x}, t)$, as well as in amplitude, $a(\mathbf{x}, t)$, such that

$$u'(\mathbf{x}, t) = a(\mathbf{x}, t) \cos [k_0 x - \omega_0 t + p_m(\mathbf{x}, t)], \tag{1}$$

where $a(\mathbf{x}, t) = a_0(\mathbf{x}) + a_m(\mathbf{x}, t)$, and $a_m(\mathbf{x}, t)$ and $p_m(\mathbf{x}, t)$ are the slowly varying amplitude and phase of an instability wave with wavenumber k_0 and frequency ω_0. Kim *et al.* (1980) have also shown that when finite-amplitude effects produce a flow with a nonlinear dispersion relation, amplitude modulation will induce phase modulation, and vice versa.

The measurements reported in this paper show that the fluctuating velocity field produced by multiply interacting instabilities in a wake can be described in terms of a dominant instability mode whose amplitude and phase are simultaneously modulated by low-frequency fluctuations. No dynamical model is available for describing how simultaneous amplitude and phase modulations are produced during wake transition. However, our results indicate that amplitude and phase modulations are produced by nonlinear interactions involving a low-frequency difference mode, and suggest that this is one of the basic features that a dynamical model should account for.

2. Experimental conditions

Transition measurements were made in the two-dimensional laminar wake of a thin airfoil (maximum thickness 3 mm, length 20 cm) in a 20×20 cm square by 120 cm long test section of a low-turbulence wind tunnel. The flow along the airfoil showed no sign of boundary-layer instability. The tunnel is an open-flow once-through type with a 20:1 contraction zone, driven from the downstream end by a Roots–Connerville positive displacement pump. The test section is isolated from pump noise by a sonic throat. The residual longitudinal turbulent intensity in the test section is 0·09 % at a wind speed of 8·4 m/s. The Reynolds number of the wake immediately behind the plate was $R = 616$, when based on the frec-stream speed U_0 and the wake half-width b.

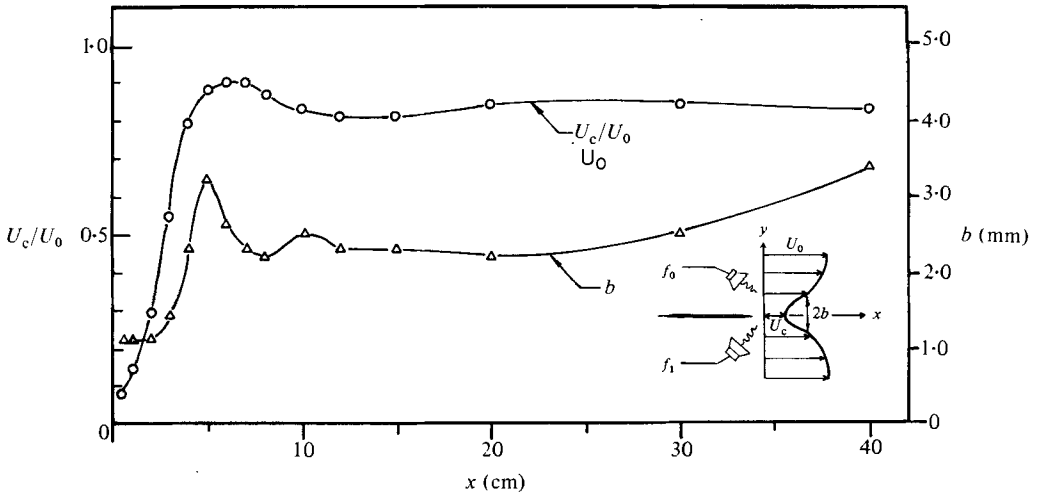

FIGURE 1. Downstream variations of centre-line velocity U_c and wake half-width b. Excitation at $f_0 = 550$ Hz and $f_1 = 582$ Hz. $U_0 = 8{\cdot}4$ m/s.

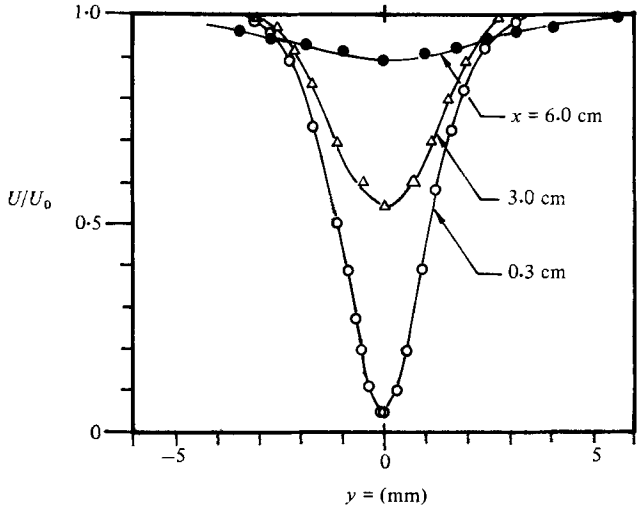

FIGURE 2. Mean-velocity distribution. $U_0 = 8{\cdot}4$ m/s. Excitation at $f_0 = 550$ Hz, and $f_1 = 582$ Hz.

The wake is symmetric, and downstream variations of centre-line velocity U_c and wake half-width b shown in figure 1 agree with the measurements of Sato & Kuriki (1961) and others. Downstream changes in mean velocity profiles formed in the wake of the splitter plate are shown in figure 2. Measurement of mean and fluctuating velocities were made with a DISA 55M constant-temperature hot-wire system. Hot-wire signals were digitized, after anti-alias filtering with Krohn–Hite filters, by a Biomation 8100 waveform recorder, which records 2048 eight-bit samples. The sampling interval was 200 μs, yielding a Nyquist frequency of 2·5 kHz. The digitized data were transferred to magnetic tape by using an LSI-11 microcomputer. Data analysis took place on the CDC Cyber 70 Model 750 computers of the University of Texas Computation Center.

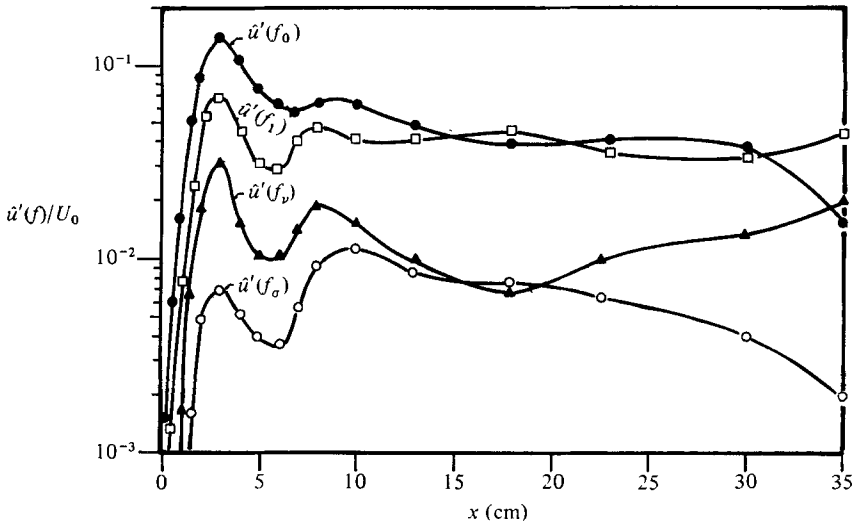

FIGURE 3. Downstream variations in the r.m.s. amplitude $\hat{u}'(f)/U_0$ of the longitudinal velocity fluctuations at the cross-stream location of peak $\hat{u}'(\mathbf{x}, t)$. $\hat{\alpha}_* = \hat{\beta}_* = 0{\cdot}4$, $\theta_* = \frac{1}{2}\pi$. ●, $\hat{u}'(f_0)$; □, $\hat{u}'(f_1)$; ▲, $\hat{u}'(f_\nu)$; ○, $\hat{u}'(f_\sigma)$.

3. Experimental results

3.1. *Linear stage of transition*

The linear-instability stage in the present experiments was used to establish the initial conditions for the subsequent nonlinear stages. More specifically, the linear stage was used to generate instability waves with specified amplitude- and phase-modulation characteristics as input for the nonlinear stages of transition. Acoustic excitation was used to excite two small-amplitude instabilities at frequencies f_0 and f_1 which lie at or near the most-amplified mode observed during natural transition. Values of f_0 and f_1 were chosen so that the difference frequency formed by their interaction was a near-neutral mode with a frequency an order of magnitude smaller than either f_0 or f_1. The level of acoustic excitation was such that at $x = 0{\cdot}1$ cm, i.e. the beginning of the initial linear-instability stage of transition, the r.m.s. amplitudes $\hat{u}'(f_0)$ and $\hat{u}'(f_1)$ of the excited modes did not exceed the level of the dominant low-frequency background noise of the tunnel. A circumflex indicates an r.m.s. value and u' is the longitudinal velocity fluctuation.

The initial development of the transition can be followed in figure 3, which shows the downstream growth of the r.m.s. amplitudes of the f_0 and f_1 instabilities. Power spectra of longitudinal velocity fluctuations shown in figure 4 indicate that as early as $x = 0{\cdot}1$ cm, weak instabilities at f_0 and f_1 are present. The power at f_0 is nearly an order of magnitude greater than that at f_1, and both are of the same order as the peaks in the low-frequency background noise. The f_0 and f_1 instabilities initially grow exponentially with downstream distance. The non-dimensional spatial growth rate $b\alpha_i = 0{\cdot}19$ measured for the most-unstable mode f_0 is in good agreement with the value of 0·20 measured by Sato & Kuriki (1961), and with the theoretical value of 0·21 calculated by Gaster (1965). No evidence of significant interactions between f_0 and f_1 can be seen until $x \simeq 1{\cdot}0$ cm, where an emerging fluctuation at the difference frequency f_ν appears in the power spectra. Note that the various low-

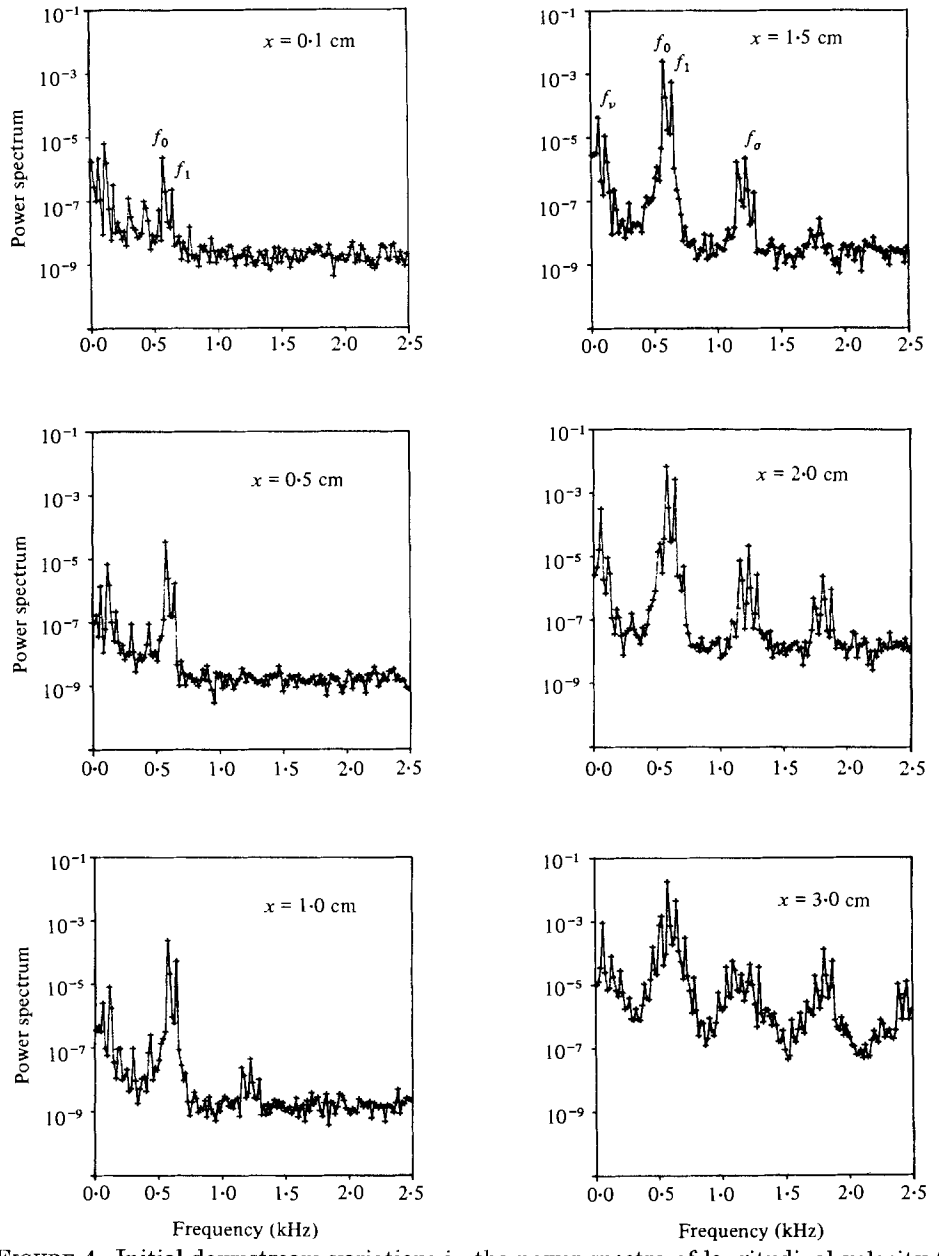

FIGURE 4. Initial downstream variations in the power spectra of longitudinal velocity fluctuations $u'^2(f)/U_0^2$. Measurements made at cross-stream points corresponding to locations of $\hat{u}'_{\max}$. $\hat{\alpha}_* = \hat{\beta}_* = 0{\cdot}4$, $\theta_* = \frac{1}{2}\pi$.

frequency spectral peaks lying between f_ν and f_0 do not grow with downstream distance from 0·1 to 1·0 cm. Rather, the peak at f_ν emerges from the naturally occurring low-frequency background noise. We shall arbitrarily refer to $x = 1{\cdot}0$ cm as the beginning of the nonlinear stage of transition, and designate it, and the transition parameters at that location, by an asterisk. In the experiments reported here, $x_* \simeq 1{\cdot}0$ cm is roughly equal to 0·7 downstream wavelengths of the dominant f_0

Experiment	Excited modes	Difference mode	AM-index α_*	PM-index β_*	Phase lag θ_*
I	$f_0 = 579$ $f_1 = 644$	$f_\nu = 65$	0·4	0·4	$\frac{1}{2}\pi$
II	$f_0 = 550$ $f_1 = 582$	$f_\nu = 32$	0·2	0·2	$\frac{1}{2}\pi$
III	$f_{-1} = 538$ $f_0 = 584$ $f_1 = 630$	$f_\nu = 46$	0·4	0·2	$-0{\cdot}2\pi$

TABLE 1

instability mode. $\hat{u}'(f_0)/U_\infty$ at this point was typically of order 1·5–2·0 %. Values of the frequency content and relative amplitudes of the instability waves at x_* are given in table 1 for the three experiments studied here. Note that, in the third experiment, three instabilities were excited in the linear stage.

The composite velocity field produced by two or more instabilities as they start to interact with one another at x_* can also be described in terms of a wave at the dominant instability frequency whose amplitude and phase are modulated by low-frequency fluctuations. We shall refer to such amplitude-modulated–phase-modulated waves as AM–PM waves. Also indicated in table 1 are the initial amplitude- and phase-modulation characteristics of the instability field at x_* as specified by the amplitude-modulation index $\hat{\alpha} = \hat{a}_m(\mathbf{x}, t)/\hat{a}_0(\mathbf{x})$, the phase-modulation index $\hat{\beta} = \hat{p}_m(\mathbf{x}, t)$, and the lag θ between the amplitude and phase modulation. The two experiments with equal amplitude- and phase-modulation characteristics at x_* (i.e. $\hat{\alpha}_* = \hat{\beta}_*$, and $\theta_* = \frac{1}{2}\pi$) represent AM–PM waves comprised of a carrier at f_0, an upper sideband at $f_1 = f_0 + f_\nu$, and a cancelled lower sideband at $f_{-1} = f_0 - f_\nu$. Primary attention will be focused on these experiments. We will also discuss some features of the transition triggered by an AM–PM wave in which the amplitude modulation ($\hat{\alpha}_* = 0{\cdot}4$) dominates the phase modulation ($\hat{\beta}_* = 0{\cdot}2$). This wave can be modelled in terms of a carrier at f_0, a weak upper sideband at $f_0 + f_\nu$, and a strong lower sideband at $f_0 - f_\nu$.

3.2. *Onset of nonlinear interactions*

At $x = 1{\cdot}00$ cm, the power spectra in figure 4 indicate that the power in the $f_0 = 579$ Hz mode is nearly an order of magnitude greater than that of the $f_1 = 644$ Hz instability, and two orders of magnitude greater than that of the emerging fluctuation at $f_\nu = f_1 - f_0 = 65$ Hz. Definite peaks at harmonic frequencies $2f_0$, $2f_1$, and the sum frequency $f_\sigma = f_0 + f_1$ also appear at $x = 1{\cdot}0$ cm, and by $x = 2{\cdot}0$ cm the dominant instability fluctuation, f_0, as well as its harmonics $2f_0$, $3f_0$, and the difference frequency f_ν have developed multiple sideband structures. Note how the generation of sidebands causes a filling in of the valleys in the spectrum. This is especially evident between $x = 2{\cdot}0$ cm and $x = 3{\cdot}0$ cm. Beyond $x_* = 1{\cdot}0$ cm, both instabilities continue to grow at their exponential rates near their initial values, even though interactions between the f_0 and f_1 instabilities become progressively stronger. As shown in figure 3, the r.m.s. amplitudes of the sum and difference modes f_σ and f_ν grow in tandem with the f_0 and f_1 instabilities. At $x = 3{\cdot}00$ cm, where the f_0 and f_1 instabilities reach a temporary finite-amplitude equilibration, the sum and difference modes also peak out.

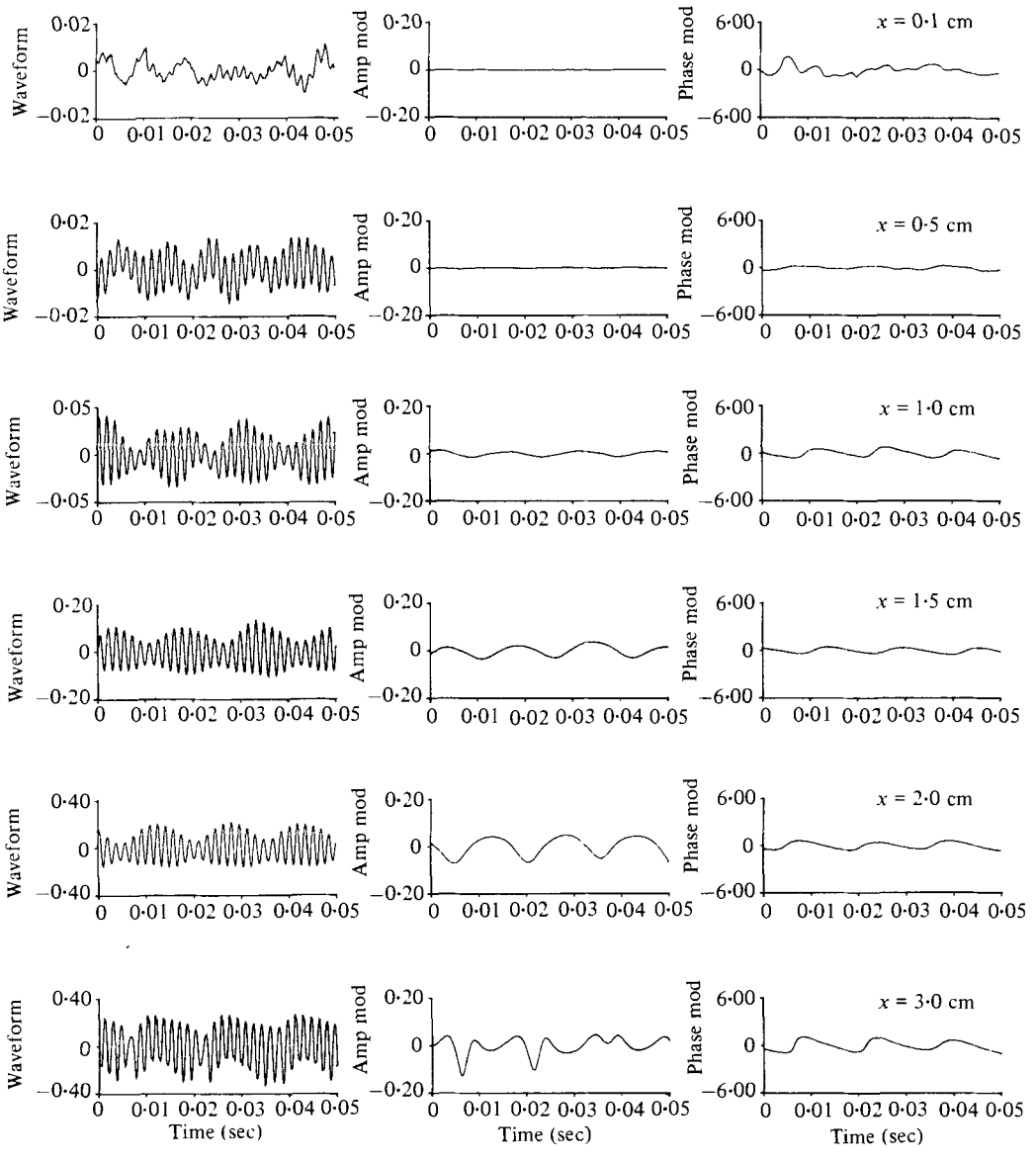

FIGURE 5. Initial downstream variations in (*a*) the waveforms of longitudinal velocity fluctuations $u'(\mathbf{x}, t)/U_0$; (*b*) the instantaneous amplitude modulation $a_m(\mathbf{x}, t)/U_0$; (*c*) the instantaneous phase modulations $p_m(\mathbf{x}, t)$, in radians, of the waveforms. Measurements correspond to the power spectra shown in figure 4. $\hat{\alpha}_* = \hat{\beta}_* = 0{\cdot}4$, $\theta_* = \frac{1}{2}\pi$.

3.3. *Downstream generation of amplitude and phase modulation*

Two notable features of the power spectra in figure 4 are the emergence of difference mode fluctuations and the generation of sideband structures. At $x = 1{\cdot}0$ cm, for example, a small but distinct fluctuation at the difference frequency is evident. At $x = 1{\cdot}5$ cm, the difference mode emerges as the dominant low-frequency fluctuation, along with a small but distinct peak at the lower sideband frequency $f_{-1} = f_0 - f_\nu$. By

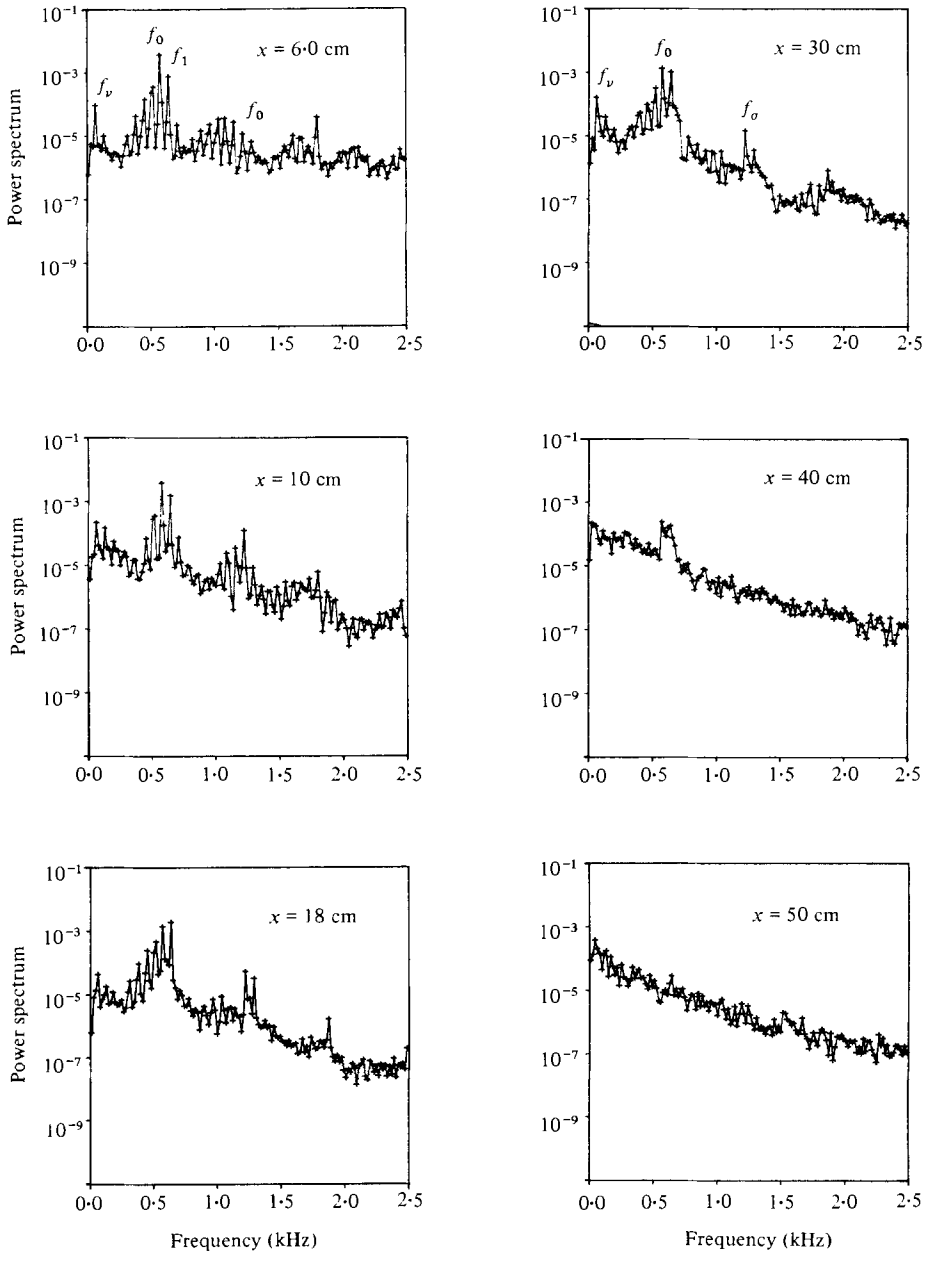

FIGURE 6. Subsequent downstream variations in the power spectra of longitudinal velocity fluctuations $u'^2(f)/U_0$. Measurements made at cross-stream points corresponding to locations of $\hat{u}'_{\max}$. $\delta_* = \beta_* = 0{\cdot}4$, $\theta_* = \frac{1}{2}\pi$. The y-locations of $\hat{u}_{\max}$ are given below:

x (cm)	y (mm)	x (cm)	y (mm)	x (cm)	y (mm)
0·1	0·3	2·0	0·6	18	3·9
0·5	0·4	3·0	1·1	30	4·2
1·0	0·4	6·0	1·9	40	3·6
1·5	0·5	10	4·1	50	0·0

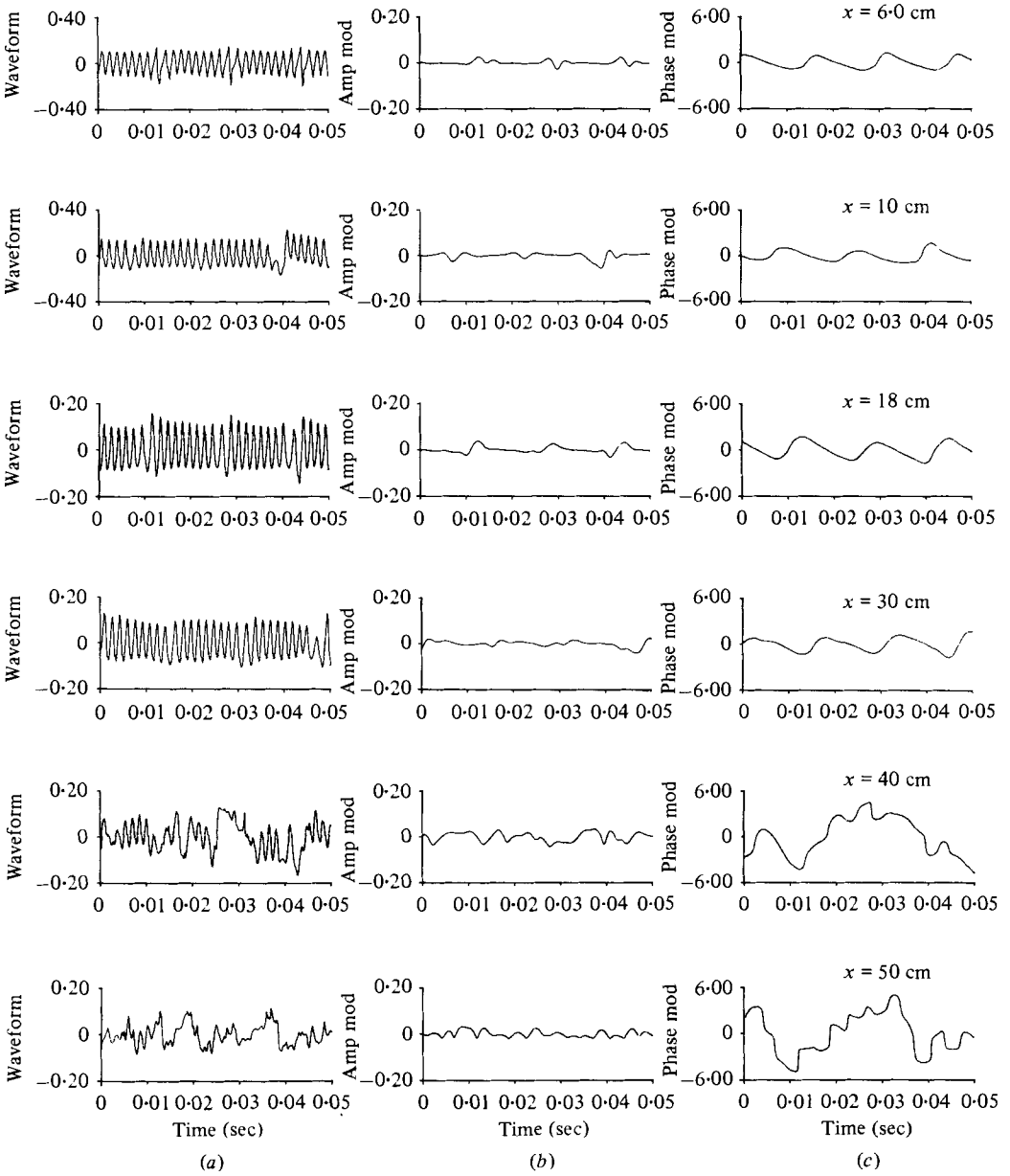

FIGURE 7. Subsequent downstream variations in (*a*) the waveforms of longitudinal velocity fluctuations $u'(\mathbf{x}, t)/U_0$; (*b*) the instantaneous amplitude modulation $a_m(\mathbf{x}, t)/U_0$; (*c*) the instantaneous phase modulations $p_m(\mathbf{x}, t)$, in radians, of the waveforms. Measurements correspond to the power spectra shown in figure 6. $\hat{\alpha}_* = \hat{\beta}_* = 0{\cdot}4$, $\theta_* = \frac{1}{2}\pi$.

$x = 2{\cdot}0$ cm, the fluctuation at f_{-1} together with the f_1 instability, which now acts like $f_{+1} = f_0 + f_\nu$, the first upper sideband, forms an asymmetric distribution of sidebands surrounding f_0. The asymmetry is even more evident if one notes the presence of fluctuations at $f_{+2} = f_0 + 2f_\nu$. By $x = 3{\cdot}0$ cm, the power spectrum displays a pronounced, asymmetrically distributed, multiple-sideband structure surrounding f_0,

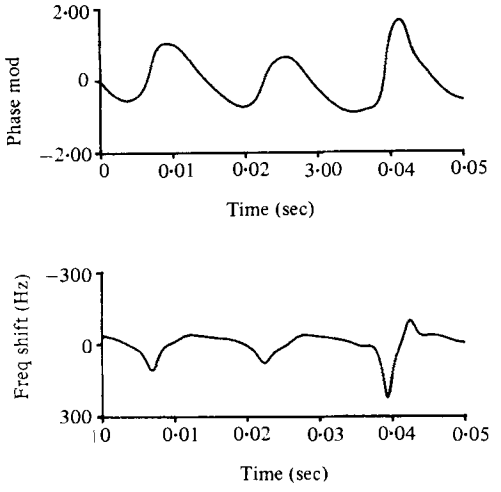

FIGURE 8. Instantaneous frequency shifts (modulations) produced by phase modulations at $x = 10{\cdot}0$ cm. The phase-modulation ordinate is in radians, while the frequency modulation ordinate is in hertz. Note that the maximum instantaneous frequency deviation in this record is of order 200 Hz, roughly 30 % of the carrier frequency f_0.

and f_ν, $2f_0$, $3f_0$, etc. As pointed out by Mollo-Christensen & Ramanonjiarisoa (1979) and others, such multiple-sideband distributions are suggestive of waves modulated in both amplitude and phase.

Shown in figure 5 are the u' velocity fluctuation waveforms corresponding to the power spectra in figure 4. The initial fluctuation field at $x = 0{\cdot}1$ cm is irregular and has no obvious regular modulations to it. As the f_0 and f_1 instabilities grow to amplitudes significantly greater than that of the background noise, the waveform starts to display a low-frequency modulation. By $x_* = 1{\cdot}0$ cm the waveform is clearly amplitude-modulated. As interactions between the f_0 and f_1 instabilities become more intense, the modulation characteristics of the waveform change. This is easily seen by comparing the waveform at $x = 3{\cdot}0$ cm with that at $x = 1{\cdot}0$ cm. It is not evident from a purely visual inspection of the modulated waveforms, however, whether modulations in phase, or equivalently in frequency, are also present. In order to obtain *quantitative* measures of the amplitude and phase modulation, the digital complex demodulation procedures of Khadra *et al.* (1981) were applied to the time-series data shown in figure 5 to compute the instantaneous amplitude and phase modulations of the waveforms. The results are shown to the right of each waveform. The instantaneous amplitude-modulation traces are plotted in the same units used for the total instantaneous waveform. The instantaneous phase-modulation scale is in units of radians. The modulation plots and the wave-form plots use the same time scale.

It is evident from figure 5 that the two growing instabilities form an amplitude-*and* phase-modulated wave at $x_* = 1{\cdot}0$ cm. Both modulations are, for the most part, sinusoidal at frequency f_ν. As transition proceeds downstream beyond $x = 3{\cdot}0$ cm, the power spectra in figure 6 and waveforms and demodulates in figure 7 indicate that amplitude modulations become irregular and weak, while phase modulations, in contrast, become stronger and more sinusoidal. Just prior to randomization and turbulence, the phase modulation becomes very intense, and contains lower frequencies.

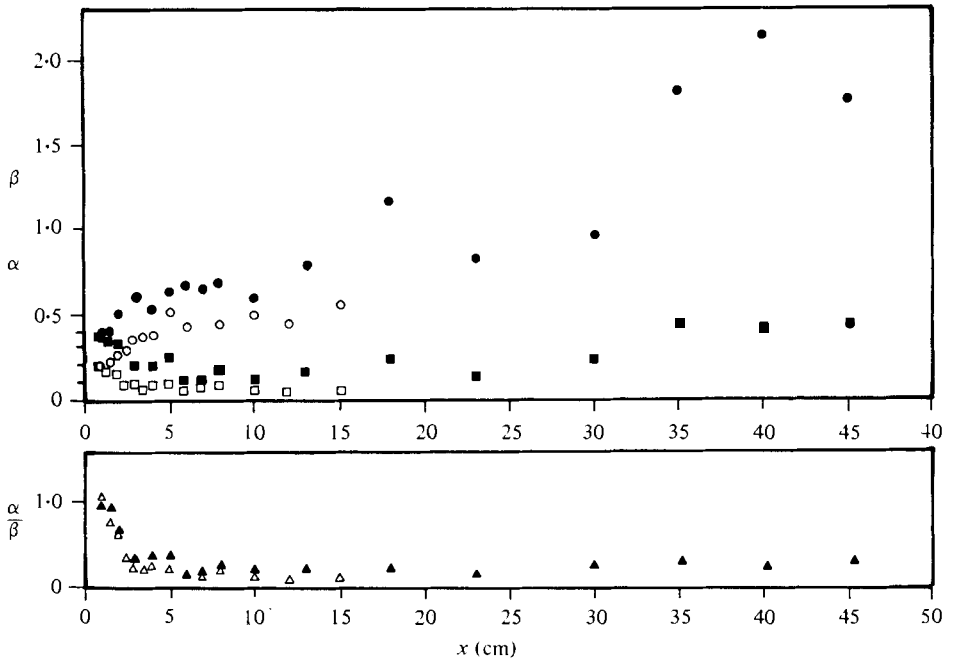

FIGURE 9. Downstream variations in the amplitude-modulation index $\hat{\alpha}$, and in the phase modulation index $\hat{\beta}$, for the longitudinal velocity fluctuations shown in figures 5 and 7. ●, $\hat{\alpha}$; ■, $\hat{\beta}$; ▲, $\hat{\alpha}/\hat{\beta}$; $\hat{\alpha}_* = \hat{\beta}_* = 0{\cdot}4$, $\theta_* = \frac{1}{2}\pi$. ○, $\hat{\alpha}$; □, $\hat{\beta}$; △, $\hat{\alpha}/\hat{\beta}$; $\hat{\alpha}_* = \hat{\beta}_* = 0{\cdot}2$, $\theta_* = \frac{1}{2}\pi$.

The basic sinusoidal nature of the phase modulation, and the frequency modulations it induces, are apparent in figure 8, where the phase modulations at $x = 10$ cm are plotted on an expanded scale. Note that the instantaneous frequency shift of the modulated wave is given by $\delta\omega(x,t) = -\partial p_m/\partial t$.

Quantitative measures of changes in the intensity of the amplitude and phase modulation were obtained by calculating the amplitude- and phase-modulation indices $\hat{\alpha}$ and $\hat{\beta}$. For the case of a wave whose phase is modulated by a single spectral component, the ratio of the maximum frequency deviation (from the carrier) to the modulation frequency is given by $\delta\omega_{\max}/\nu = \beta$. Computed downstream variations in $\hat{\alpha}$, $\hat{\beta}$ and $\hat{\alpha}/\hat{\beta}$ are plotted in figure 9. Note that, initially at $x_* = 1{\cdot}0$ cm, $\hat{\alpha}$ and $\hat{\beta}$ have the same value,

$$\hat{\alpha}_* = \hat{\beta}_* \simeq 0{\cdot}4,$$

indicating that the instability wave in this experiment starts out with equal amplitude- and phase-modulation characteristics. However, strong nonlinear activity within the first 3–5 cm of downstream distance (i.e. roughly 2–3 wavelengths of f_0) causes $\hat{\alpha}$ to rapidly decrease to a value of roughly 0·10, while $\hat{\beta}$, in contrast, increases to a value of roughly 0·6, giving a value of $\hat{\alpha}/\hat{\beta} = 0{\cdot}16$. Between $5 < x < 30$ cm, both $\hat{\alpha}$ and $\hat{\beta}$ stay fairly constant in value. The mean velocity deficit and wake half-width shown in figure 2, as well as peak values of $\hat{u}'(f_0)$ and $\hat{u}'(f_1)$ shown in figure 3, also stay fairly constant in this region. For $x > 30$ cm, the power spectra in figure 6 indicate a rapid evolution to a turbulent spectrum. This final randomization stage is accompanied by a marked increase in the phase-modulation index $\hat{\beta}$ in figure 9. Also shown in figure 9 are values of $\hat{\alpha}$, $\hat{\beta}$ and $\hat{\alpha}/\hat{\beta}$ measured in a similar series of experiments in which

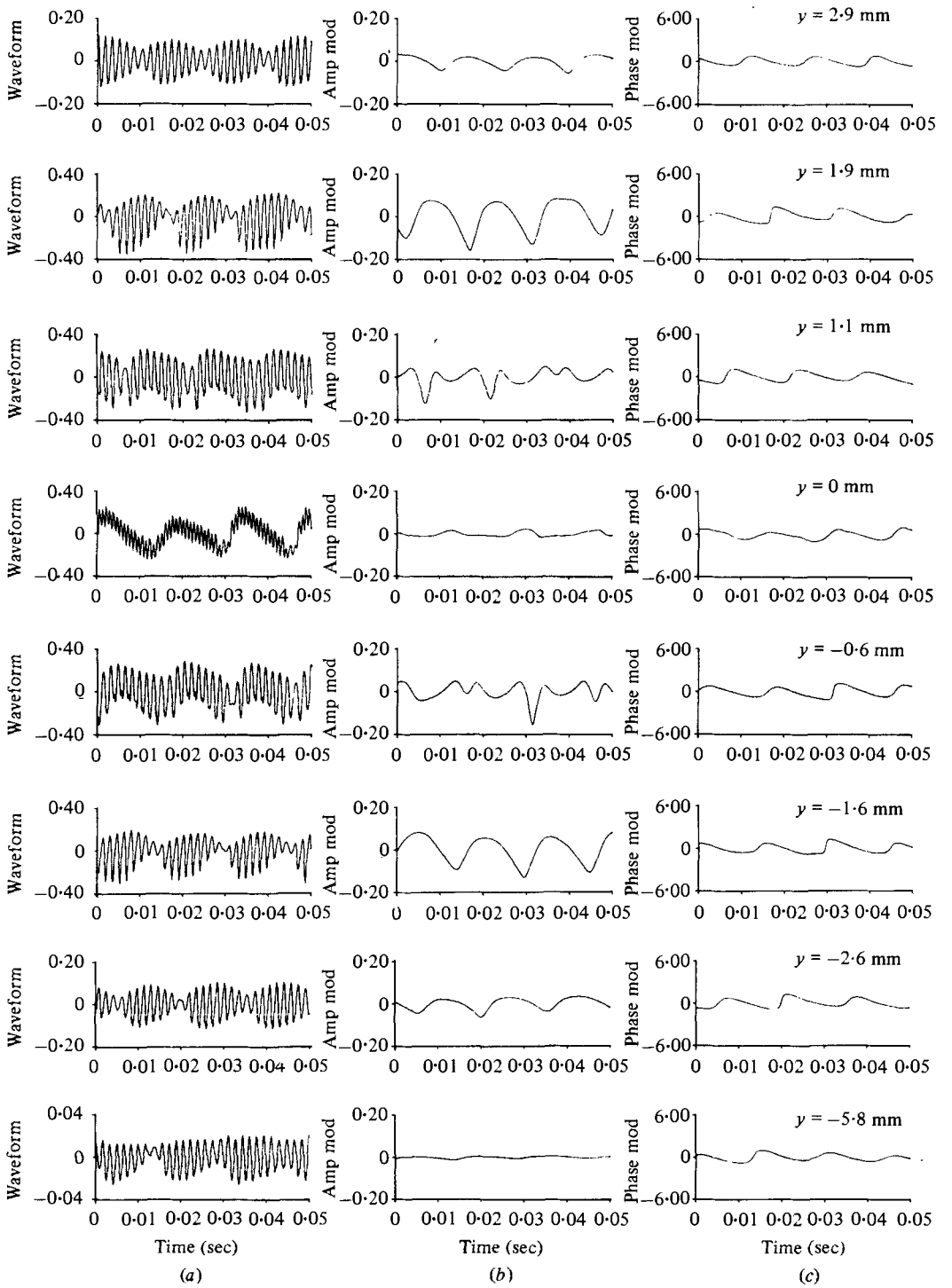

FIGURE 10. Cross-stream variations in (*a*) the waveforms of longitudinal velocity fluctuations $u'(\mathbf{x}, t)/U_0$; (*b*) the instantaneous amplitude modulation $a_m(\mathbf{x}, t)/U_0$; (*c*) the instantaneous phase modulations $p_m(\mathbf{x}, t)$, in radians, of the waveforms at $x = 3{\cdot}00$ cm. $\hat{\alpha}_* = \hat{\beta}_* = 0{\cdot}4$, $\theta_* = \frac{1}{2}\pi$.

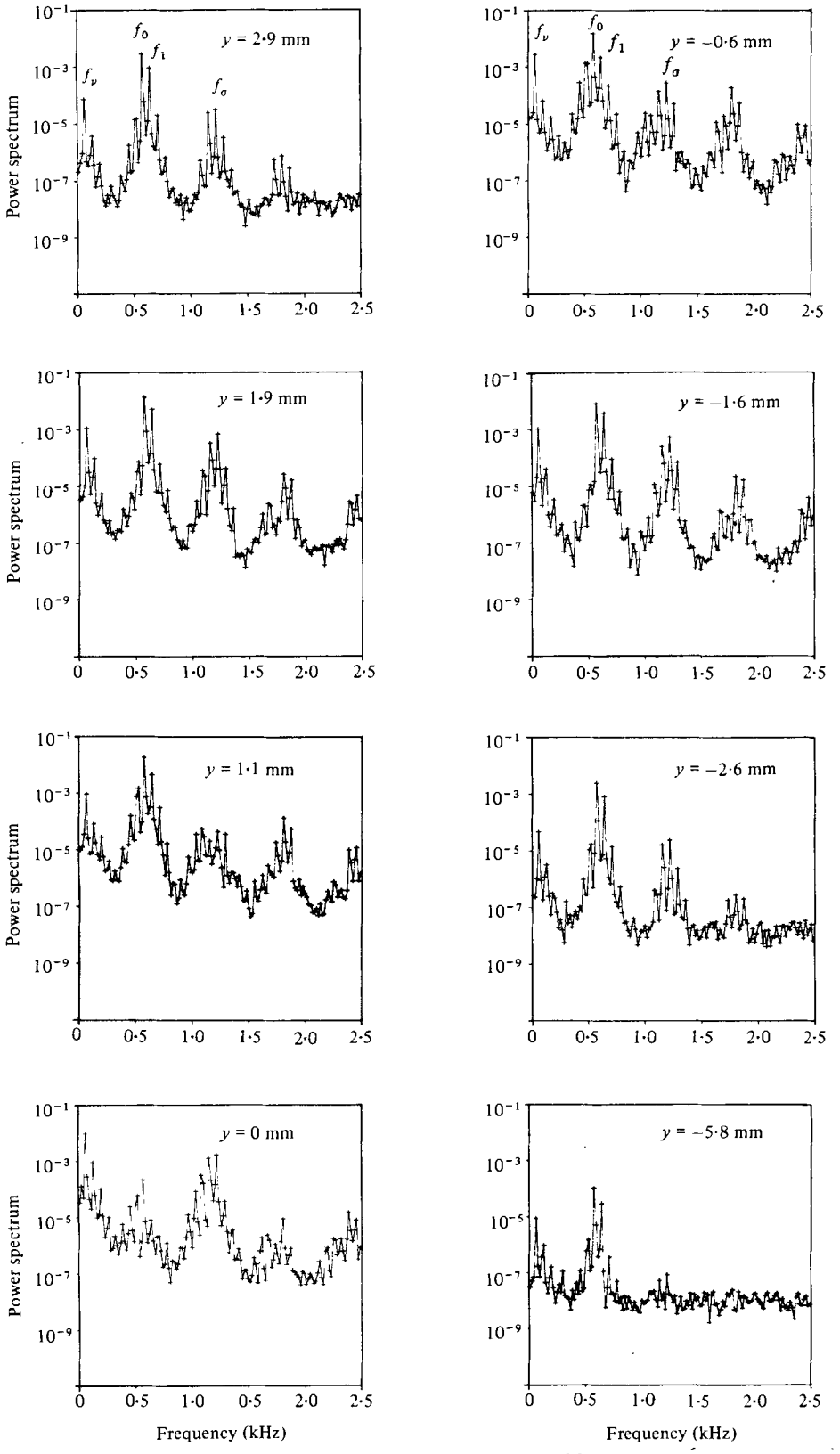

FIGURE 11. Cross-stream variations in the power spectra of longitudinal velocity fluctuations $u'^2(f)/U_0^2$ at x = 3·00 cm. Measurements correspond to the waveforms in figure 10. $\alpha_* = \beta_* = 0{\cdot}4$, $\theta_* = \frac{1}{2}\pi$.

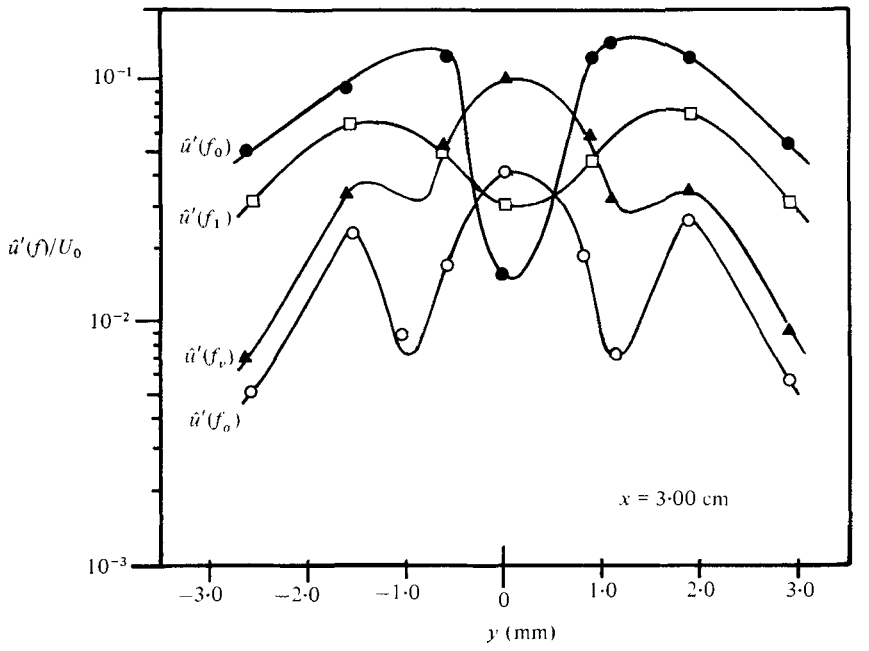

FIGURE 12. Cross-stream variations in the r.m.s. amplitude of longitudinal velocity fluctuations $\hat{u}'(f)$ at x = 3·00 cm. ●, $\hat{u}'(f_0)$; □, $\hat{u}'(f_1)$; ▲, $\hat{u}'(f_\nu)$; ○, $\hat{u}'(f_\sigma)$. $\hat{\alpha}_* = \hat{\beta}_* = 0{\cdot}4$, $\theta_* = \frac{1}{2}\pi$.

$\hat{\alpha}_* = \hat{\beta}_* = 0{\cdot}2$ and $\theta_* = \frac{1}{2}\pi$ at $x_* = 1{\cdot}0$ (see table 1). Although the initial modulation levels differ, the same basic tendency for phase modulation to dominate the highly nonlinear stages of transition is apparent.

3.4. *Cross-stream variations in amplitude and phase modulations*

Measured cross-stream variations in the instability waveforms and power spectra are shown in figures 10 and 11 for velocity fluctuations measured at x = 3·00 cm, the location of the downstream maximum in $\hat{u}'(f_0)$ shown in figure 3. Cross-stream waveforms show pronounced changes in the amplitude-modulation characteristics as y varies from the centre line of the wake. At the $y = 0$ centre line, for example, the f_0 instability mode and its sidebands are weak and the spectrum is dominated by large-amplitude fluctuations at f_ν and $2f_0$; note the harmonics of f_ν and the sidebands around $2f_0$. As distance from the centre line increases, power spectra show that the energy at f_ν decreases, while that at f_0 increases until a maximum is reached at y = 1·1 cm, after which it decreases. Cross-stream variations in power spectra reflect the influence of cross-stream modal structure of the various fluctuations. Cross-stream r.m.s. profiles at x = 3·0 cm are plotted in figure 12. The difference and sum frequency modes have maximum values at the centre line, while the f_0 and f_1 instability modes have off-axis peaks.

The amplitude- and phase-modulation time traces of the waveforms in figure 10 are plotted to the right of the corresponding time traces. They reveal a high degree of cross-stream variability in amplitude modulation. At the centre line, for example, virtually no amplitude modulation is present, even though strong low-frequency fluctuations are evident in the total waveform and in the power spectra. In

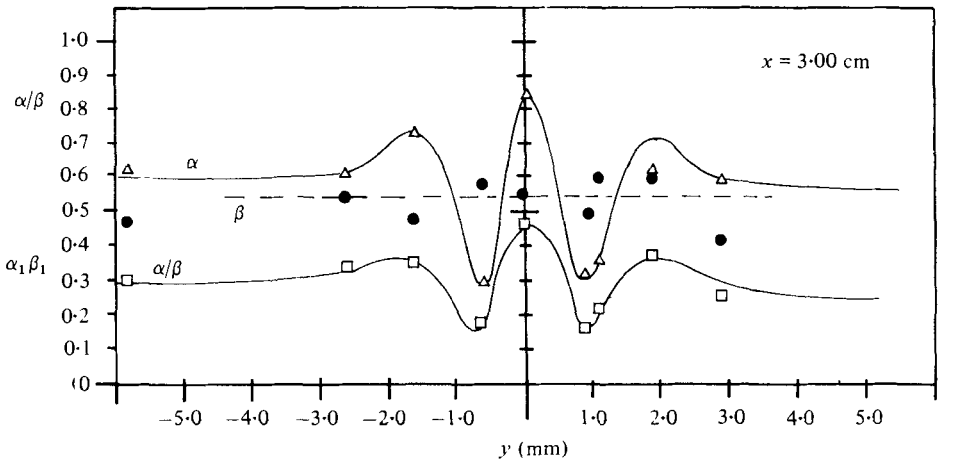

FIGURE 13. Cross-stream variations in the amplitude-modulation index $\hat{\alpha}$, and in the phase modulation index $\hat{\beta}$, for the longitudinal velocity fluctuations shown in figure 10. $x = 3{\cdot}00$ cm. △, $\hat{\alpha}$; ●, $\hat{\beta}$; □, $\hat{\alpha}/\hat{\beta}$. $\hat{\alpha}_* = \hat{\beta}_* = 0{\cdot}4$, $\theta_* = \frac{1}{2}\pi$.

contrast, at $y = 1{\cdot}1$ cm, the location of the maximum value of $\hat{u}'(f_0)$, very strong amplitude modulations are evident. Cross-stream changes in phase modulation are much less pronounced. Strong, basically sinusoidal, phase modulations are evident in figure 10 at all cross-stream locations. Cross-stream variations in the amplitude- and phase-modulation indices are plotted in figure 13. Note the non-zero value for the amplitude-modulation index $\hat{\alpha}$ at the centre line. This is a result of the definition of the modulation index which requires the small degree of amplitude modulation to be normalized by the equally small r.m.s. value of the f_0 fluctuations at the centre line.

3.5. *Variations in sideband distribution asymmetry*

A notable feature of the power spectra plotted in figures 4, 6 and 11 is a tendency for the asymmetry of the distribution of sidebands $f_0 \pm nf_\nu$ to change with both downstream distance and cross-stream location. The symmetry or asymmetry of the distribution of sidebands relative to the 'carrier' is related to the degree of amplitude and phase modulations as measured by α and β, and to the phase lag θ between the amplitude and phase modulations. This is most readily apparent when the modulations are sinusoidal and of the same frequency. Modulation time traces indicate that, for a substantial portion of the nonlinear stages of transition, the low-frequency modulations are close in many cases to being single-frequency sinusoids. Some useful insight can be gained by comparing experimental results with the analytic features of a wave at (ω_0, k_0) whose amplitude and phase are modulated by a single low-frequency wave at (ν, κ):

$$u'(x,t) = a_0[1 + \alpha \sin(\kappa x - \nu t + \theta)] \cos[k_0 x - \omega_0 t + \beta \sin(\kappa x - \nu t)]. \tag{2}$$

The phase lag between the amplitude and phase modulation is given by θ. As shown by Kim *et al.* (1980), this modulated wave is equivalent to a 'carrier' wave centred at (ω_0, k_0), surrounded by 'sideband' fluctuations at frequencies $\omega_n = \omega_0 \pm n\nu$ and wavenumbers $k_n = k_0 + n\kappa$:

$$u'(x,t) = a_0 \sum_{n=-\infty}^{\infty} A_n \cos(k_n x - \omega_n t + \phi_n). \tag{3}$$

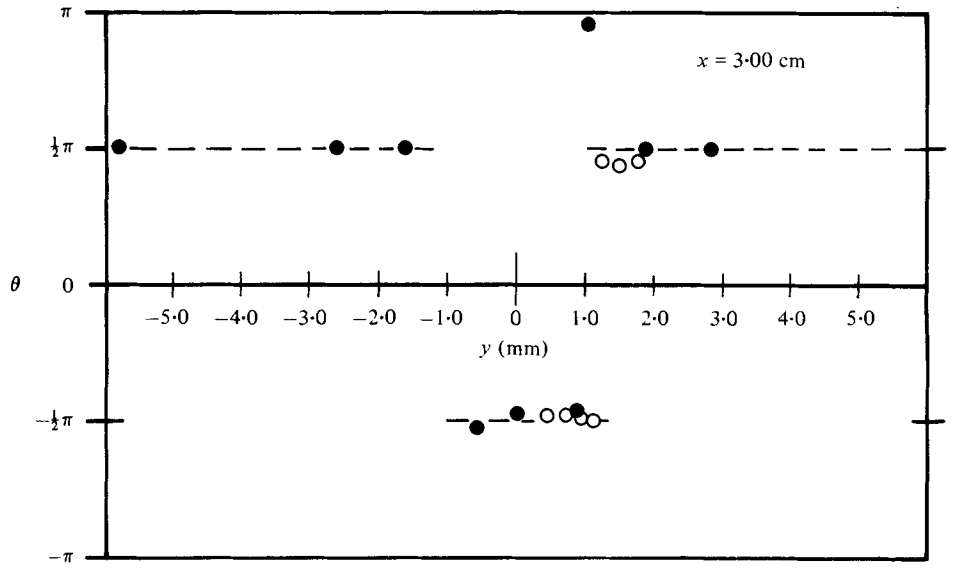

FIGURE 14. Cross-stream variations in θ, the phase lag between the amplitude and phase modulation, of the longitudinal velocity fluctuations shown in figures 10 and 11 at $x = 3{\cdot}00$ cm. ●, values of θ measured for $\hat{\alpha}_* = \hat{\beta}_* = 0{\cdot}4, \theta_* = \frac{1}{2}\pi$. ○, values of θ measured for $\hat{\alpha}_* = \hat{\beta}_* = 0{\cdot}2$, $\theta_* = \frac{1}{2}\pi$.

The power difference between the nth upper and lower sidebands is determined by

$$A_n^2 - A_{-n}^2 = \frac{4\alpha n}{\beta} J_n^2(\beta) \sin\theta, \tag{4}$$

where $\alpha = \sqrt{2}\,\hat{\alpha}$, $\beta = \sqrt{2}\,\hat{\beta}$, and $J_n(\beta)$ is the Bessel function of the first kind.

Values of α and β therefore determine the magnitude of the power difference between the nth upper and lower sidebands. However, it is the value of θ, the phase lag between amplitude and phase modulation, which determines the sign of the difference; i.e. the sense of the asymmetry of sideband distribution relative to the carrier. For $\theta = 0$, the distribution will be symmetric. When the amplitude modulation and phase modulation are out of phase by $-\frac{1}{2}\pi$, the lower sidebands are larger than the upper sidebands, and the distribution will be skewed towards the lower sidebands. When $\theta = \frac{1}{2}\pi$, the upper sidebands are larger than the lower sidebands, and the asymmetry will be skewed towards the upper sidebands.

The connection between sideband asymmetry and phase lag θ can be seen by comparing the cross-stream values of θ, plotted in figure 14 for $x = 3{\cdot}00$ cm, with cross-stream changes in sideband distribution shown in figure 11. Cross-stream values of θ vary from $+\frac{1}{2}\pi$ for $|y| > 1{\cdot}1$ cm to $-\frac{1}{2}\pi$ for $|y| < 1{\cdot}1$ cm. The location $|y| \simeq 1{\cdot}1$ cm at which θ changes sign coincides with the peak in $\hat{u}'(f_0)$ shown in figure 13. Note that for $|y| > 1{\cdot}1$ cm the symmetry of sideband distribution is skewed towards the upper sidebands, while for $|y| < 1{\cdot}1$ cm the sidebands are skewed towards the lower sidebands. Near $|y| \simeq 1{\cdot}1$ cm, the sidebands are symmetrically distributed and θ appears to go through a zero axis crossing.

When considering the meaning of changes in sideband asymmetry, it is important to keep in mind that the values of θ computed by digital complex demodulation are

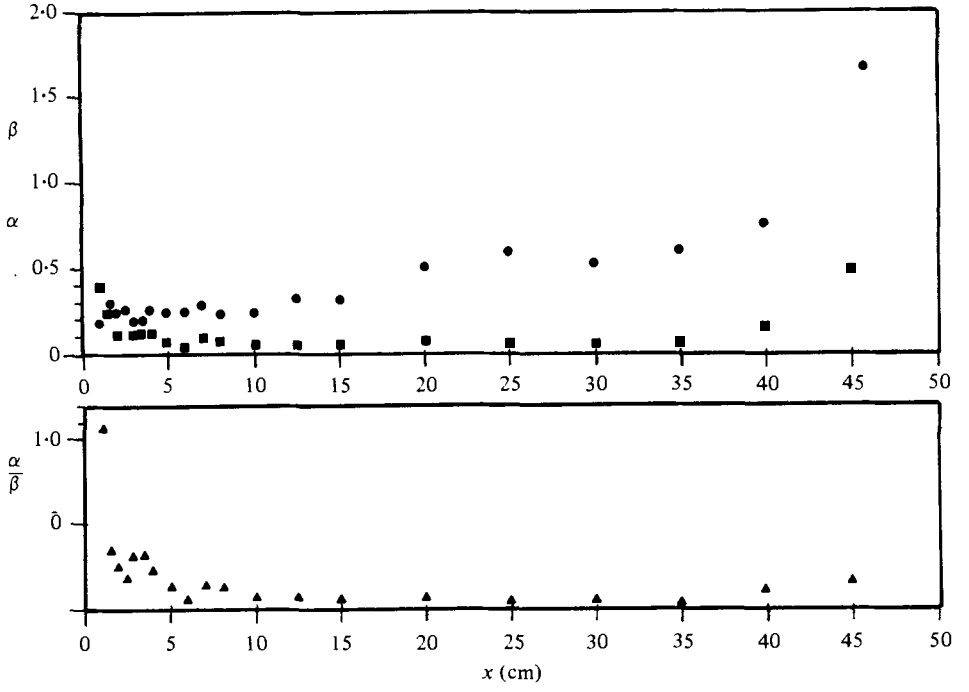

FIGURE 15. Downstream variations in the amplitude-modulation index $\hat{\alpha}$, and in the phase-modulation index $\hat{\beta}$, for longitudinal velocity fluctuations when $\hat{\alpha}_* = 0{\cdot}4, \hat{\beta}_* = 0{\cdot}2, \theta_* = -0{\cdot}2\pi$. Values of $\hat{\alpha}$ and $\hat{\beta}$ measured at cross-stream locations where $S_u = E[u'(x,t)^2]^{\frac{1}{2}}$ is a maximum. ●, $\hat{\beta}$; ■, $\hat{\alpha}$; ▲, $\hat{\alpha}/\hat{\beta}$.

determined by the sideband structure of the modulated wave being analysed. In other words, if a wave with a particular sideband distribution is analysed by digital complex demodulation, then values of α, β and θ will be computed which give the 'equivalent' AM–PM description of that wave. Thus changes in amplitude and phase modulation can be viewed as an alternative way to describe changes in the distribution and energy content of the sideband structure.

4. Discussion

4.1. *Spectral broadening and energy redistribution by modulation*

The results presented so far demonstrate that the fluctuating velocity field observed in the nonlinear stages of multiple-instability transition can be described in terms of an amplitude- and phase-modulated wave at the dominant instability frequency. The amplitude and phase modulations are at frequencies corresponding to that of the difference mode f_ν and its harmonics. As downstream distance increases, and spectral broadening becomes more pronounced, phase modulation as measured by $\hat{\beta}$ becomes more intense, and amplitude modulation as measured by $\hat{\alpha}$ becomes less intense. The ratio $\hat{\alpha}/\hat{\beta}$ decreases rapidly in both experiments. The general connection between spectral broadening and changes in phase modulation is not unique to transitions with equal amplitude- and phase-modulation indices at the onset of nonlinear activity. For example, shown in figure 15 is the downstream behaviour of $\hat{\alpha}$, $\hat{\beta}$ and $\hat{\alpha}/\hat{\beta}$ for an AM–PM wave that is initially dominated by amplitude modulations such that

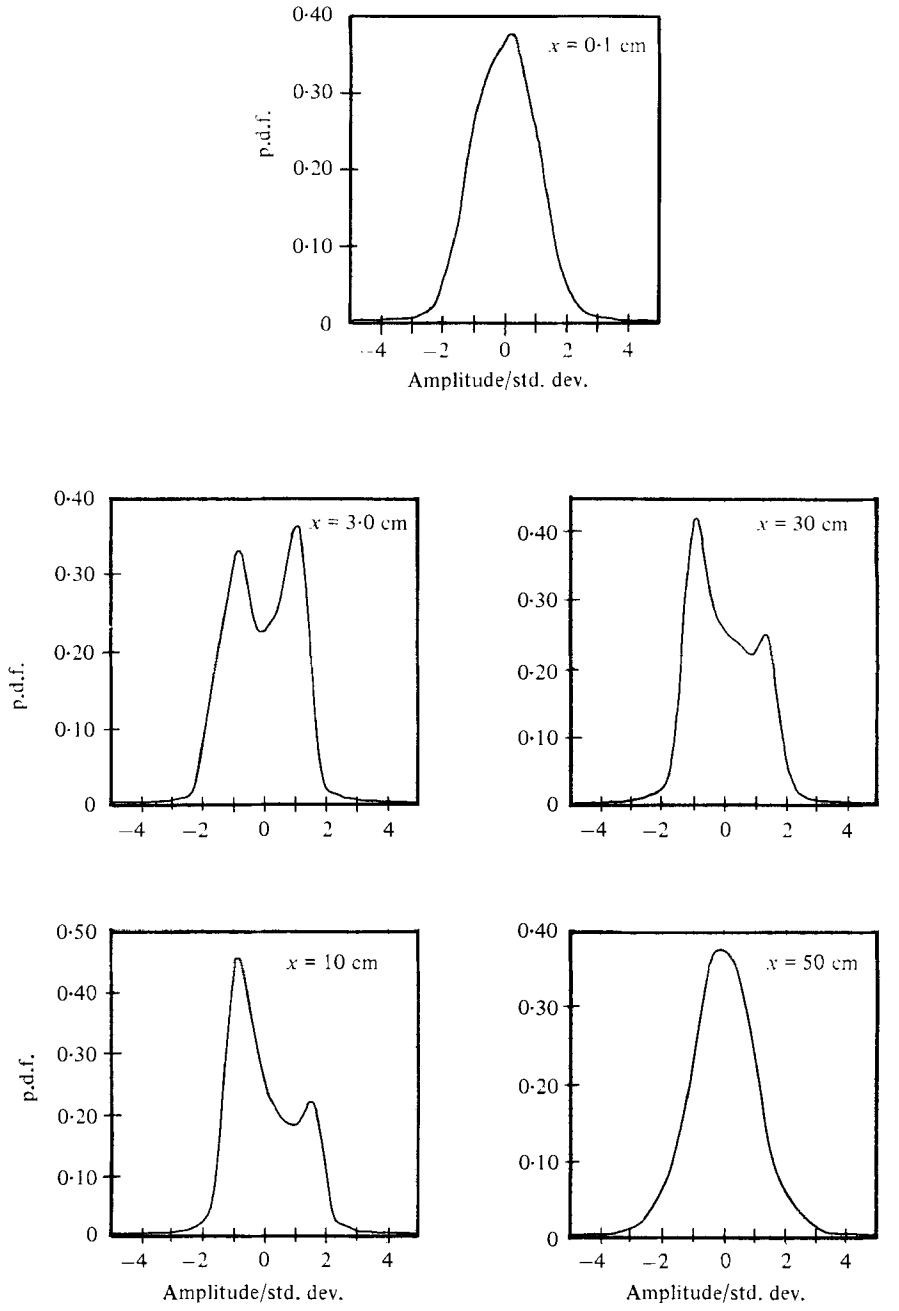

FIGURE 16. Downstream changes in the probability density function (p.d.f.) of longitudinal velocity fluctuations at cross-stream locations of $\hat{u}'_{max}$. P.d.f. values calculated by the procedure of Tarter & Kranmal (1967). $\hat{\alpha}_* = \hat{\beta}_* = 0{\cdot}4$, $\theta_* = \frac{1}{2}\pi$.

$\hat{\alpha}_* = 0{\cdot}4$, $\hat{\beta}_* = 0{\cdot}2$ and $\theta_* = -0{\cdot}2\pi$. Although there are detailed differences in how $\hat{\alpha}$ and $\hat{\beta}$ behave in this experiment, the same general trends are observable; namely the amplitude-modulation index decreases and the phase-modulation index increases as transition progresses. Thus, even when transition is provided with an AM–PM wave that is dominated by amplitude modulation, it chooses to enhance the phase-modulation characteristics of the fluctuating velocity field.

The spectral broadening and randomization role of phase modulation becomes even more apparent when downstream changes in $\hat{\alpha}$ and $\hat{\beta}$ are compared with downstream changes in the probability density function (p.d.f.) of longitudinal velocity fluctuations (figure 16). Initially, at the onset of instability, $x = 0{\cdot}1$ cm, the wake is laminar and the low-intensity random background fluctuations display a gaussian-like distribution. The onset of instability effectively organizes the flow by introducing a narrow band of intense fluctuations which receive energy directly from the mean flow. By $x = 3{\cdot}0$ cm, the velocity field exhibits the statistical characteristics of a dominant instability wave superimposed on a field of random background fluctuations. As transition progresses, nonlinear interactions redistribute instability-mode energy by producing sidebands and low-frequency difference modes, and the p.d.f. becomes skewed by $x = 10$ cm. In the strong spectral-broadening region $10 < x < 40$ cm, where $\hat{\beta}$ remains relatively constant, the p.d.f. changes only slightly. However, beyond $x = 40$ cm, where $\hat{\beta}$ changes dramatically, the flow evolves into a final turbulent state with a much higher random-fluctuation energy level, and the p.d.f. takes on a gaussian-like distribution characteristic of turbulent flow.

The question of interest then is why transition apparently prefers to emphasize phase modulation instead of amplitude modulation. Some simple considerations based on general properties of amplitude- and phase-modulated waves suggest that the preference may be due to the more efficient spectral-energy redistribution properties of phase-modulated waves (Panter 1965). For example, consider a wave at f_0 whose amplitude is modulated by a simple sinusoidal fluctuation at f_ν (i.e. let $\beta = 0$ in (2)). This pure amplitude-modulation process will yield only two new sidebands, at $f_0 \pm f_\nu$, the sum and difference frequencies. In contrast, set $\alpha = 0$ and consider a wave at f_0 whose phase is modulated by a simple sinusoidal at f_ν. This purely phase-modulated wave will yield, strictly speaking, an infinite number of sidebands at $f_0 \pm nf_\nu$ ($n = 1, 2, \ldots$). The number of sidebands with significant amplitudes, and the size of the frequency shifts from the carrier, will increase as the phase-modulation index β increases. A more significant difference between amplitude and phase modulation, however, is the fact that simple amplitude modulation cannot alter (redistribute) the energy of the carrier wave. For example, although phase modulation generates numerous sidebands, the total energy of a phase-modulated wave remains constant at $\frac{1}{2}a_0^2$. To achieve this, the energy of the carrier wave decreases, as determined by its coefficient $J_0^2(\beta)$, so that the residual energy can be distributed to its sidebands. In contrast, although the total energy in a purely amplitude-modulated wave increases over that of an unmodulated wave, the energy of the carrier is unaffected and remains at $\frac{1}{2}a_0^2$; the added energy a_m^2, supplied by the modulated wave, finds its way into the sidebands only. If, as generally suspected, the spectral redistribution of energy is one of the primary roles of nonlinear interactions, then simple amplitude modulation cannot get the job done effectively since it cannot redistribute the energy of the dominant instability wave. Phase modulation, however, can redistribute carrier

energy. The efficiency of the redistribution, as measured by the number of sidebands generated and their amplitudes, increases as the phase-modulation index increases, just as observed in our experimental data.

Although phase modulation dominates the downstream transition, our measurements show that simultaneous amplitude modulations are still present, and are presumably available to play a role in the transition. The particular nature of that role is suggested by the spectral composition and power of a wave with simultaneous amplitude and phase modulations. As shown by Panter (1965), when the amplitude and phase of a wave are simultaneously modulated, the energy of the carrier wave, as well as that of the amplitude-modulating wave, can be redistributed to the sidebands. The efficiency of the redistribution depends on the phase-modulation index β, while the added energy which can be redistributed, along with that of the carrier, depends on the amplitude modulation. Since amplitude modulations will always exist when waves interact, it appears that one of the major roles amplitude modulation may play in transition is that of a provider of energy for phase modulation to redistribute to the sidebands.

As transition proceeds downstream, the power spectra in figures 4 and 6 indicate that nonlinear interactions produce more and more low-frequency fluctuations which can participate in the modulation process. The velocity waveforms and modulation time traces in figures 5 and 7 show that the low-frequency fluctuations become more irregular. Note how the phase modulations become very intense and very low in frequency during the randomization stage. The efficiency of spectral broadening and randomization is enhanced in multitone phase-modulated waves (or in amplitude-multitone phase-modulated waves) by the production of cross-product sidebands due to intermodulations. Cross-product sidebands are not produced by multitone amplitude modulation. For example, if amplitude modulations $a_{m1}(t) = \alpha_1 \cos(\nu_1 t + \theta_1)$ and $a_{m2}(t) = \alpha_2 \cos(\nu_2 t + \theta_2)$ give rise to sidebands at $\omega_0 \pm \nu_1$ and $\omega_0 \pm \nu_2$ respectively, then the multitone amplitude modulation $a_m(t) = a_{m1}(t) + a_{m2}(t)$ will only give rise to sidebands at $\omega_0 \pm \nu_1$ and $\omega_0 \pm \nu_2$. In contrast, if sinusoidal phase modulations

$$p_{m1}(t) = \beta_1 \sin(\nu_1 t + \phi_1) \quad \text{and} \quad p_{m2}(t) = \beta_2 \sin(\nu_2 t + \phi_2)$$

give rise to sidebands at

$$\omega_0 \pm n\nu_1 \quad \text{and} \quad \omega_0 \pm m\nu_2 \quad (n, m = 1, 2, 3, \ldots),$$

the multitone modulation

$$p_m(t) = p_{m1}(t) + p_{m2}(t)$$

will give rise to sidebands at

$$\omega_0 + n\nu_1 + m\nu_2 \quad (n, m, = \pm 1, \pm 2, \ldots).$$

In addition, when combined amplitude and multitone phase modulation occurs, the phases of the variously generated sidebands will be of the form $\pm m_1\phi_1 \pm m_2\phi_2 - \theta_1$, and any randomness associated with either the amplitude modulation or the phase modulation will be efficiently spread throughout the spectrum.

4.2. *Nonlinear interactions and the production of phase and amplitude modulations*

The simple properties of amplitude- and phase-modulated waves just presented do not provide a physical model for the spectral-broadening process. They do suggest, however, why our data indicates the importance of phase modulations in the transition process. The question remains as to how amplitude and phase modulations are

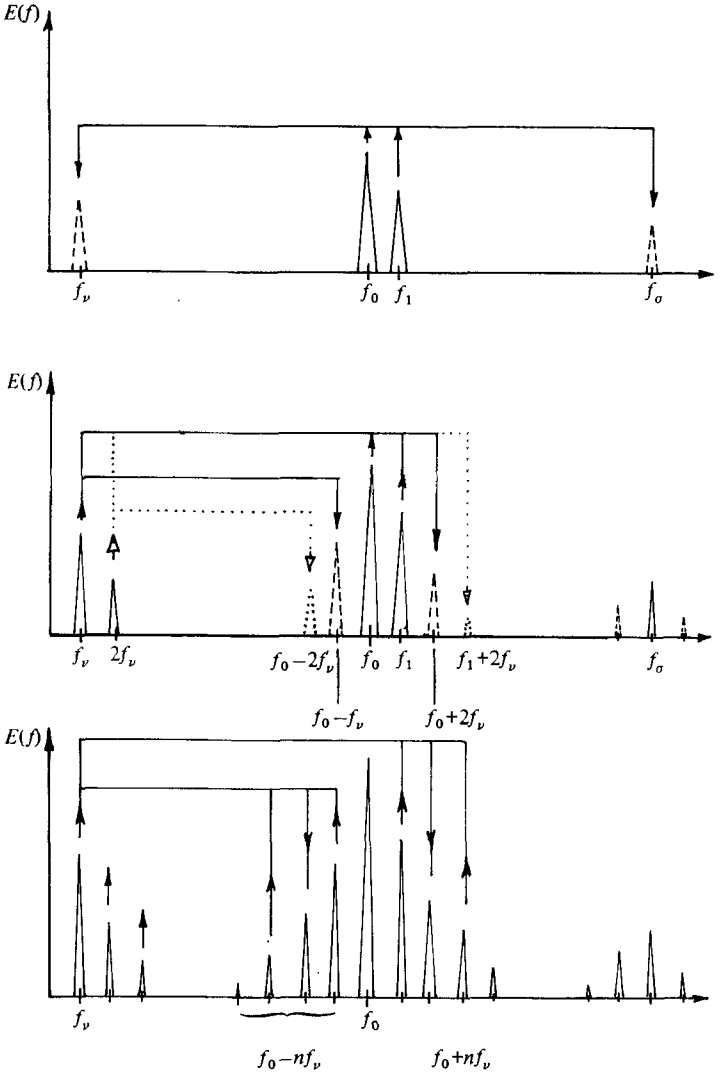

FIGURE 17. Schematic of AM–PM sideband production by three-wave coupling interactions.

generated. Our results and those of Motohashi (1979) indicate that the emergence of a strong low-frequency velocity fluctuation at the difference frequency plays a significant role in initiating the generation of amplitude and phase modulations, and in producing subsequent modulation changes as transition progresses. The picture that emerges from experimental measurements is that amplitude and phase modulations may be generated by a process, illustrated in figure 17, that goes somewhat as follows. Natural modes f_0 and f_1 of the wake are excited and grow exponentially. After attaining finite, but small, amplitudes, f_0 and f_1 interact nonlinearly to produce sum- and difference-frequency modes f_σ and f_ν. The difference-frequency mode grows exponentially (but not at a rate predicted by linear theory) and subsequently interacts with the two instability modes to produce other sum and difference modes. These modes appear as 'sidebands' of the most-unstable instability mode. This process continues

as the transition progresses towards turbulence and subsequent multiple cross-interactions produce a continuous evolution of the transition spectrum.

4.2.1. *Bicoherency spectrum.* Some features of this descriptive picture can be substantiated by using measurements of the bicoherency spectrum to detect the presence of nonlinearly interacting waves. As shown in a series of papers by Kim & Powers 1978, 1979; Kim *et al.* 1980), the bicoherency spectrum is defined as

$$b^2(\omega_i, \omega_j) = \frac{|B(\omega_i, \omega_j)|^2}{E|\Phi(\omega_i)\,\Phi(\omega_j)|^2\, E|\Phi(\omega_i+\omega_j)|^2}. \tag{5}$$

$\Phi(\omega_i)$ represents the computed Fourier amplitude of the velocity fluctuation time series at position (x, y) in the flow, and E denotes an expected value. The bispectrum is

$$B(\omega_i, \omega_j) = E[\Phi(\omega_i)\,\Phi(\omega_j)\,\Phi(\omega_i+\omega_j)].$$

The bicoherence spectrum measures the coherence between three waves due to nonlinear coupling. The bicoherency spectrum is bounded by

$$0 \leqslant b^2(\omega_i, \omega_j) \leqslant 1.$$

Values of the bicoherency near unity indicate that the wave at $\omega_m = \omega_i + \omega_j$ is excited by the coupling (interaction) of waves at ω_i and ω_j. A value of the bicoherency near zero implies an absence of phase coherence and suggests that even though the waves at ω_i, ω_j, and ω_m may satisfy the resonant frequency matching condition $\omega_m = \omega_i + \omega_j$, they are not coupled and the fluctuation at ω_m is not the result of interactions between fluctuations at ω_i and ω_j. It can also be shown that the value of $b^2(\omega_i, \omega_j)$ provides a measure of the fraction of power at $\omega_i + \omega_j$ due to nonlinear coupling of the waves at ω_i and ω_j.

The bicoherency spectrum was computed for the velocity fluctuation fields measured at $x = 2$ cm, 3 cm and 6 cm in the experiments where $\hat{\alpha}_* = \hat{\beta}_* = 0{\cdot}4$ and $\theta = \frac{1}{2}\pi$. The y-co-ordinates correspond to locations where $\hat{u}'$ is a maximum. The spectra at these locations are given in figures 4 and 6. It is clear from figures 1, 3 and 9 that the region $2{\cdot}0 \leqslant x \leqslant 6$ cm is characterized by intense variations in mean-flow development, velocity-fluctuation growth and modulation-index ratio change. Values of the bicoherence were computed by the digital bispectral analysis techniques of Kim & Powers (1978). An ensemble of 16 statistically independent records was created by measuring the fluctuating velocity field during intervals formed by randomly turning the excitation oscillators on and then off. This procedure insured that each measurement was statistically uncorrelated with the others, and allowed us to detect any phase coherence among wave triads due to nonlinear coupling.

4.2.2. *Sum and difference mode production.* Computed bicoherency spectra are plotted in figure 18. Note that, as early as $x = 2{\cdot}0$ cm, significant peaks ($b^2 \geqslant 0{\cdot}90$) appear at frequency pairs corresponding to the difference interaction $b^2(f_\nu, f_0)$ and to the sum interaction $b^2(f_0, f_1)$, providing quantitative evidence that the fluctuations which fall at the difference and sum frequencies are indeed due to the interaction of the f_0 and f_1 modes. The high values of squared bicoherency measured for the sum and difference interactions indicate that the major fraction of power of the fluctuations at f_ν and f_σ is due to nonlinear coupling of the fluctuations at f_0 and f_1. Although the sum interaction has a larger value of squared bicoherency than the difference interaction, power-spectra measurements show that it is the difference mode that grows most

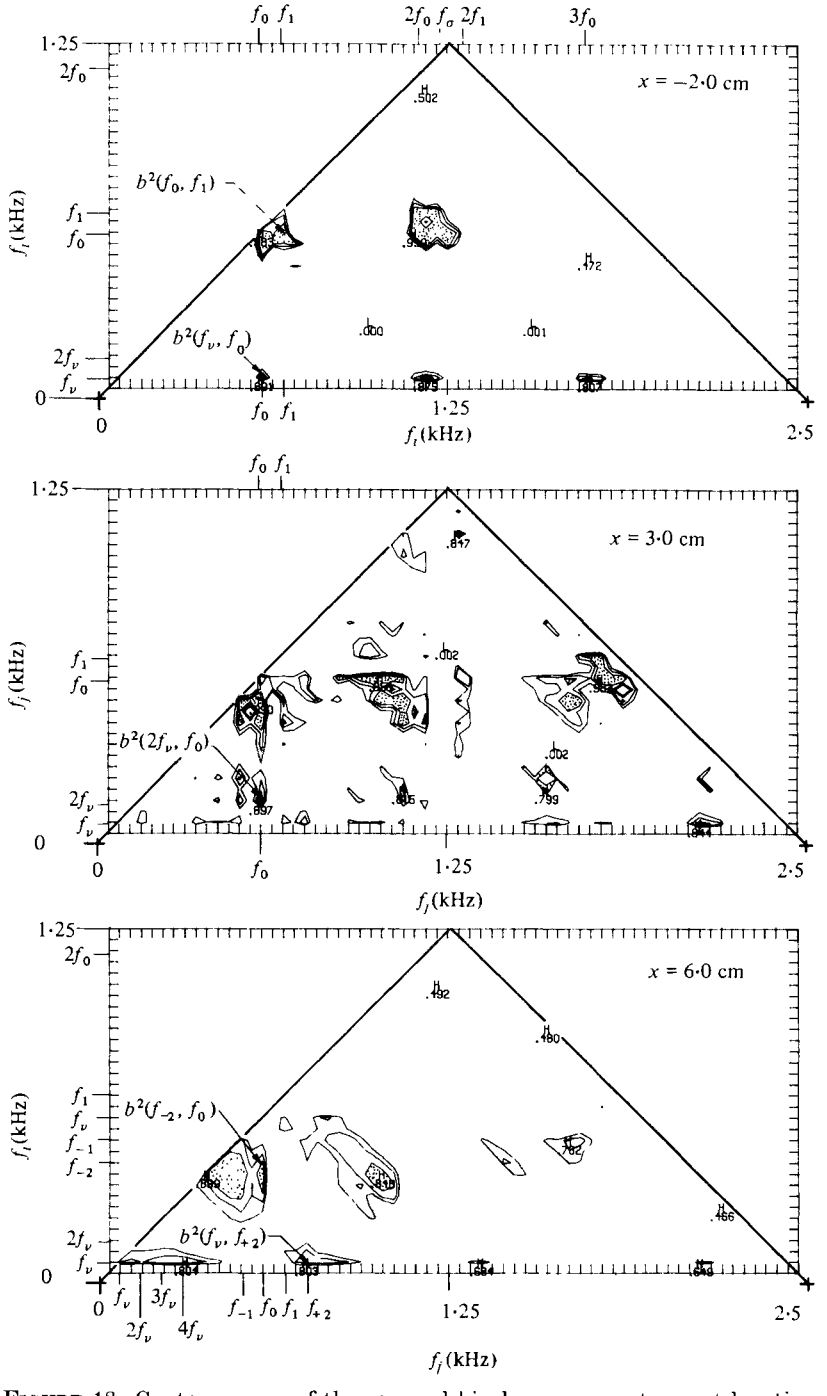

FIGURE 18. Contour maps of the squared bicoherency spectrum at locations of $\hat{u}'_{\max}$. Contour levels are at $b^2(f_i, f_j) = 0{\cdot}6$, $0{\cdot}7$ and $0{\cdot}8$. $\hat{\alpha}_* = \hat{\beta}_* = 0{\cdot}4$, $\theta_* = \frac{1}{2}\pi$.

(f_i, f_j)	$b^2(f_i, f_j)$ $x = 2{\cdot}0$ cm	$x = 3{\cdot}0$ cm	$x = 6{\cdot}0$ cm
(f_ν, f_0)	0·89	0·56	0·57
(f_0, f_1)	0·98	0·68	0·66
(f_ν, f_{-1})	0·55	0·69	0·59
$(2f_\nu, f_0)$	0·05	0·90	0·26
$(2f_\nu, f_{-2})$	0·05	0·80	0·24
$(f_\nu, 2f_0)$	0·86	0·26	0·56
$(f_\nu, 3f_0)$	0·81	0·56	0·09
$(2f_\nu, 2f_0)$	0·14	0·63	0·37
$(2f_\nu, 3f_0)$	0·09	0·55	0·06
(f_0, f_0)	0·98	0·94	0·18
$(f_0, 2f_0)$	0·94	0·66	0·25

TABLE 2

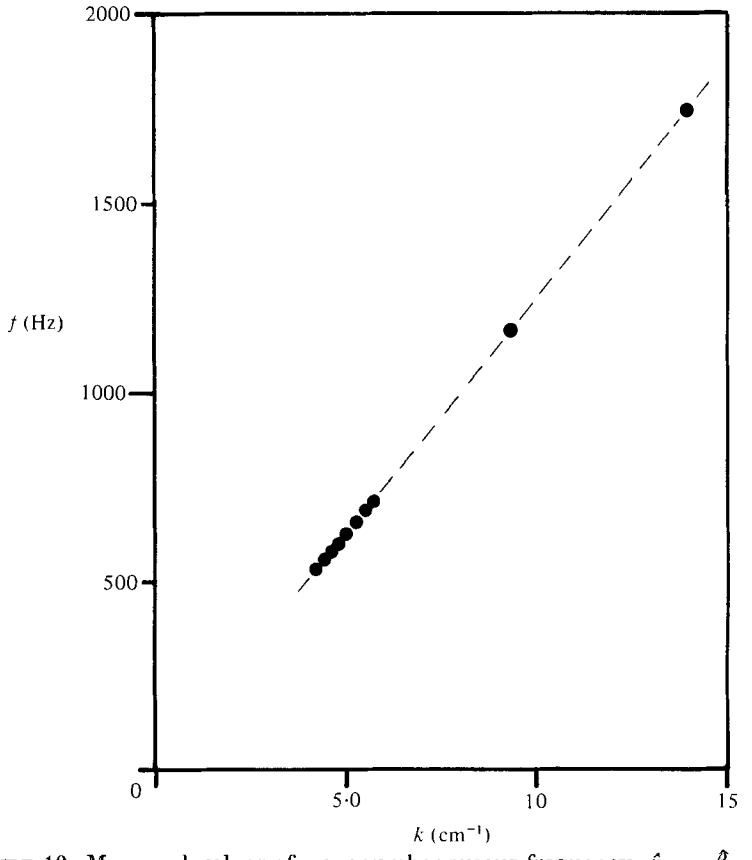

FIGURE 19. Measured values of wavenumber versus frequency. $\hat{\alpha}_* = \beta_* = 0{\cdot}2$, $\theta_* = \frac{1}{2}\pi$.

energetically. Miksad, Jones & Powers (1981) computed the bispectral power transfer function for the interactions of f_0 and f_1 and showed that for $\hat{u}'(f_1)/\hat{u}'(f_0)$ greater than roughly 0·25 the power flow into f_ν due to nonlinear interactions between f_1 and f_0 exceeds the power flow to f_0. In the present experiments $\hat{u}'(f_1)/\hat{u}'(f_0)$ equals 0·65 at $x = 2{\cdot}00$ cm.

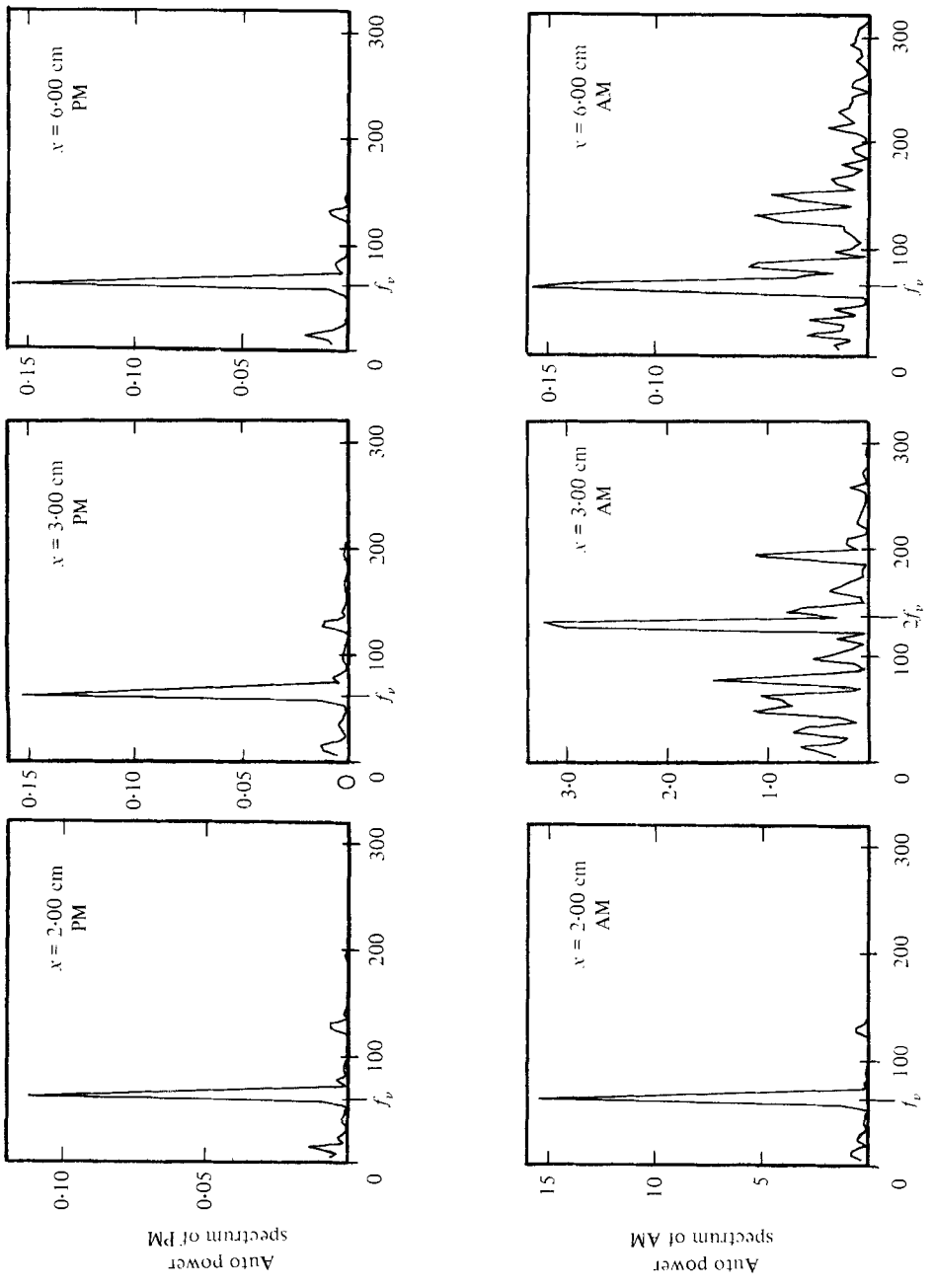

FIGURE 20. Power spectra of the instantaneous amplitude and phase modulations at the locations used to compute the squared bicoherency spectra in figure 18. $\alpha_* = \beta_* = 0{\cdot}4$, $\theta_* = \frac{1}{2}\pi$.

4.2.3. *Sideband production.* The various other bicoherency peaks in figure 18 indicate nonlinear couplings among the many modes in the transition spectrum. Some of these values are given in table 2. Of particular relevance to the production of sidebands surrounding f_0, and its harmonics, are the peaks in the bicoherency spectrum at $b^2(f_\nu,f_0)$, $b^2(f_\nu, 2f_0)$ and $b^2(f_\nu, 3f_0)$. These peaks correspond to interactions between the difference mode f_ν and the higher-frequency modes f_0, $2f_0$, and $3f_0$ to produce sideband structures of the form $f_0 \pm nf_\nu$, $2f_0 \pm nf_\nu$, etc. In comparing the bicoherency calculations at $x = 2{\cdot}0$ cm with those at $x = 3{\cdot}0$ cm, particular note should be taken of the fact that, although at $x = 3{\cdot}0$ cm bicoherency peaks are still present at $b^2(f_\nu,f_0)$, the largest sideband production peaks have moved to interactions of the form $b^2(2f_\nu, nf_0)$; i.e. interactions between $2f_\nu$ and f_0, $2f_0$ and $3f_0$. By $x = 6{\cdot}0$ cm the sideband-producing peaks again lie at $b^2(f_\nu, nf_0)$. It is not at all evident from the power spectra at $x = 3{\cdot}0$ cm why $2f_\nu$ should be preferentially involved in the production of sidebands. A component at $2f_\nu$ does appear in the spectrum at $x = 3{\cdot}0$ cm, but it is only one-half as large as the peak at f_ν. We have no explanation for this puzzling anomaly other than, as indicated in figure 18, interactions with $2f_\nu$ may be more efficient in adding widely spaced sidebands to enhance the filling of the spectral valleys to either side of the carrier.

4.2.4. *AM–PM production via nonlinear interactions.* The shift in the bicoherency peak from f_ν to $2f_\nu$ and back again, although not understood, does provide a convenient test case to examine the contention of Bakai (1970) and Kim *et al.* (1980) that the modulation characteristics of a carrier wave can be described in terms of nonlinear wave–wave interactions between a low-frequency difference wave (or one of its harmonics) and a carrier wave† and its sidebands. If this is a valid premise, then one would expect to see some sort of change in the modulation characteristics at $x = 3{\cdot}0$ cm.

Shown in figure 20 are the power spectra of amplitude and phase modulations at the three downstream locations. At $x = 2{\cdot}0$ cm, both amplitude modulation and phase modulation are dominated by the f_ν component, and the peak in the bicoherency spectrum falls at $b^2(f_\nu,f_0)$. At $x = 3{\cdot}0$ cm, however, the amplitude-modulation spectrum is dominated by a $2f_\nu$ component, and the bicoherency peak has shifted to $b^2(2f_\nu,f_0)$. In contrast, the phase-modulation spectrum is still dominated by an f_ν component, although a small peak is present at $2f_\nu$. At $x = 6{\cdot}0$ cm, the peak in the amplitude-modulation spectrum returns to $2f_\nu$, and the bicoherency returns to $b^2(f_\nu,f_0)$. The phase-modulation spectrum remains at f_ν. It is interesting to note that the amplitude modulations shown in figure 10 at $x = 3{\cdot}00$ cm exhibit second-harmonic distortions at y-locations which roughly correspond to maxima in the amplitude $\hat{u}'(f_0)$ of the dominant instability mode (figure 12). The phase-modulation time traces, on the other hand, exhibit some second-harmonic distortions near the centre line where $\hat{u}'(f_0)$ is a minimum but $\hat{u}'(f_\nu)$ is a maximum. It appears, then, that the mechanisms controlling phase and amplitude modulations may not reside at the same location in the shear layer. They do, however, seem to be linked, though not necessarily in lock-step at any particular cross-stream location.

Although distortions in amplitude modulation at $x = 3{\cdot}00$ cm appear at cross-stream locations corresponding to $\hat{u}'(f_0)$ maxima, it is clear from figure 13 that the most intense amplitude modulations, as measured by the modulation index $\hat{\alpha}$, occur at

† Wavenumber–frequency measurements shown in figure 19 indicate that f_0 and its harmonic waves at $2f_0$, $3f_0$ all travel at the same speed.

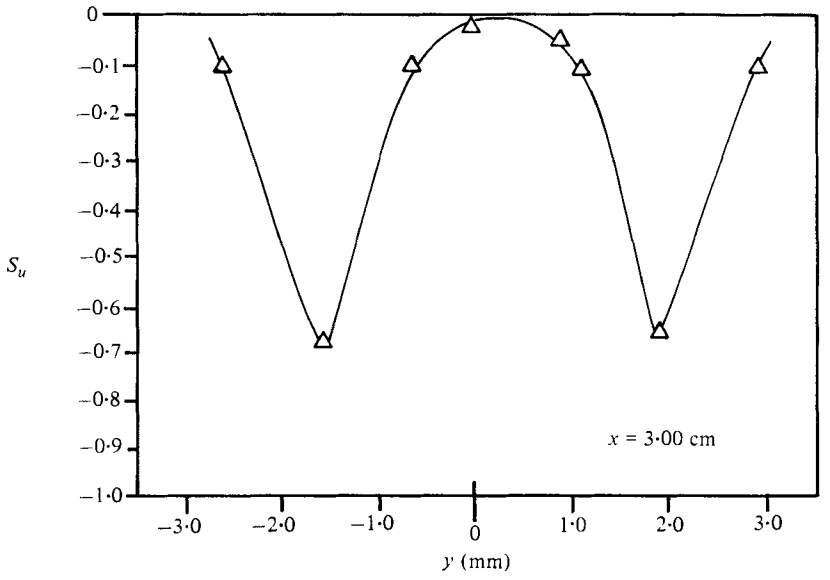

FIGURE 21. Measured cross-stream values of the skewness S_u of longitudinal velocity fluctuations at $x = 3{\cdot}00$ cm. $\hat{\alpha}_* = \hat{\beta}_* = 0{\cdot}4$, $\theta_* = \frac{1}{2}\pi$.

cross-stream locations beyond that of $\hat{u}'(f_0)$ maxima. We have shown that amplitude modulation is related to nonlinear interactions. The strength of these interactions can be measured by the bicoherency spectrum, $b^2(\omega_i, \omega_j)$ which is determined by the bispectrum $B(\omega_i, \omega_j)$. Kim & Powers (1979) and others have shown that the bispectrum represents the contribution to the mean-cube value of the fluctuation velocity field $E[u'(x,t)^3]$ due to the interaction of those spectral components at ω_i and ω_j. A normalized mean-cube value, the skewness, can be defined as $S_u = E[u'^3]/E[u'^2]^{\frac{3}{2}}$.

Measured cross-stream values of S_u are plotted in figure 21 for $x = 3{\cdot}00$ cm. Note that the maximum negative values of the mean-cube value occur at cross-stream locations which correspond closely to the cross-stream locations of maximums in the amplitude-modulation index (figure 13). As noted earlier, the large centre-line values of α do not seem to have dynamic significance. They occur because of the definition $\alpha = a_m/a_0$, and reflect the fact that a_0 is very small at the centre-line. Although the amplitude-modulation index α is sensitive to the cross-stream values of S_u, the phase-modulation index β stays relatively constant across the shear layer.

It appears, then, that amplitude modulation is intimately connected with the local cross-stream and downstream details of the nonlinear interactions which take place during transition. Phase modulations, on the other hand, exhibit both cross-stream and downstream memory. The two types of modulations are clearly linked in some manner, by the nonlinear dynamics of the transition. We suspect that the phase modulations are controlled by the largest-amplitude low-frequency fluctuation; perhaps by a parametric effect set up by low-frequency periodic distortions of the mean shear. The link between amplitude and phase modulations seems to be the result of the nonlinear interactions that produce the low-frequency fluctuations, which once generated interact back with the instability modes to produce low-frequency amplitude modulations.

4.2.5. *AM–PM and nonlinear dispersion.* A simple argument by Kim *et al.* (1980)

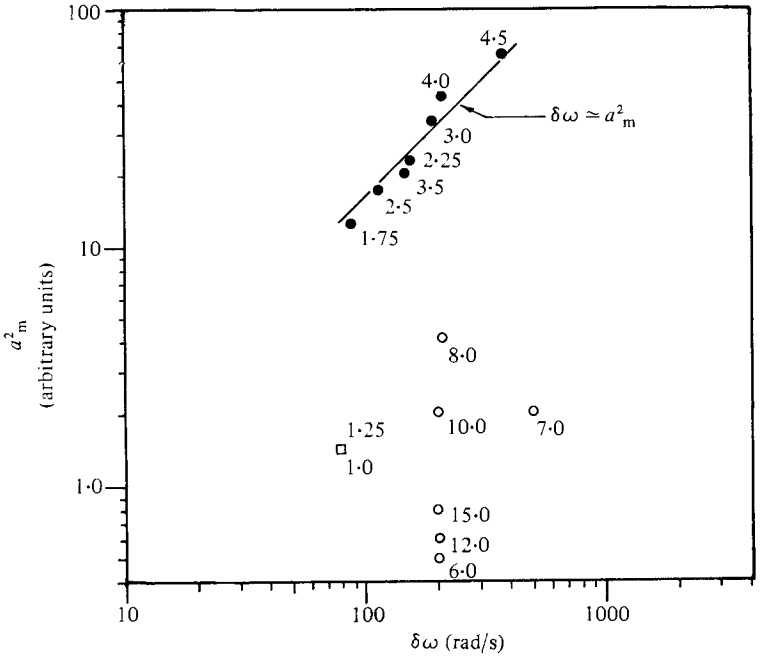

FIGURE 22. Downstream variations in the frequency deviation $\delta\omega$ relative to the carrier versus the magnitude squared of the amplitude modulation (arbitrary units) for the velocity fluctuations shown in figures 5 and 7. The slope of the solid line is unity.

(which does not consider local variations in flow dynamics) does show that a link can exist between amplitude and phase modulations when finite-amplitude effects produce a dispersion relation of the form $\omega = \omega(k, a^2)$. Using the notation of (1), it is fairly straightforward to show that if the modulation amplitude $a_m(x,t)$† is small compared with $a_0(x)$, then the instantaneous frequency of the wave can be expressed as

$$\omega = \omega_0(k) + (\partial\omega/\partial a^2)_{a_0}\delta a^2(x,t),$$

where $\delta a^2 = a_m^2(x,t)$. We can regard $\omega - \omega_0(k) = \delta\omega$ as the local time variation of wave frequency due to finite-amplitude effects. Since the instantaneous frequency of the modulated wave in (1) is $\omega = \omega_0 - \partial p/\partial t$, we have $\delta\omega = -\partial p_m/\partial t$ and

$$\partial p_m(x,t)/\partial t = -(\partial\omega/\partial a^2)_{a_0} a_m^2(x,t). \tag{6}$$

Thus, if finite-amplitude effects establish an amplitude-dependent dispersion relation, we find that amplitude modulation $a_m(x,t)$ can induce phase modulation $p_m(x,t)$, and vice versa. Measured values of $\delta\omega$ as a function of a_m^2 are shown in figure 22 for the $\hat{\alpha}_* = \hat{\beta}_* = 0{\cdot}2$, $\theta_* = \frac{1}{2}\pi$ experiments. The numbers next to each point indicate the downstream location of the measurement. Note that, from $x = 1{\cdot}75$ cm to $x = 5{\cdot}00$ cm, where the amplitude $\hat{u}'(f_0)/U_0$ of the dominant instability exceeds an apparent threshold value of roughly 5 % (see figure 3), $|\delta\omega|$ does indeed vary directly with a_m^2.

† The modulation amplitude $a_m(x, t)$ is not to be confused with the amplitude $u'_\nu(x, t)$ of the difference mode, even though the difference mode, through various nonlinear interactions, may be the ultimate source of $a_m(x, t)$.

For $\hat{u}'(f_0)/U_0 \lesssim 5\%$ no consistent relation between $|\delta\omega|$ and a_m^2 could be measured. This suggests that one of the primary roles of the exponentially growing instability may be to establish appropriate finite-amplitude conditions (vis-à-vis $\omega(k, a^2)$) such that any amplitude modulation produced by the onset of nonlinear interactions can induce the generation or maintenance of phase modulation.

5. Conclusions

The overall picture of transition that arises from our measurements is as follows. Small-amplitude disturbances trigger instabilities which grow exponentially in amplitude. Nonlinear interactions between growing instabilities produce sum and difference modes. Strong difference modes interact back with the dominant instabilities to produce amplitude modulations. At the same time, nonlinear dispersion effects $\omega(k, a^2)$, established by the finite amplitude of the growing instability, condition the flow so that existing amplitude modulations can trigger phase modulations. Once simultaneous phase and amplitude modulations are established, they may be maintained, or altered, by subsequent nonlinear three-wave interaction mechanisms, or by parametric effects. Our measurements indicate that the mechanism of phase modulation dominates the spectral-broadening and energy-redistribution process. Amplitude modulation seems to play the role of an energy provider.

This work was supported by the National Science Foundation under Grant MEA-7800719. The digital signal-processing techniques used in this study were developed under the auspices of the Department of Defense Joint Services Electronics Program through the Air Force Office of Scientific Research under Contract F 49620-77-C-0101.

REFERENCES

BAKAI, A. S. 1970 *Nucl. Fusion* **10**, 53.

GASTER, M. 1965 *Prog. Aero. Sci.* **6**, 251.

GERTSENSHTEIN, S. YA., SUKHORUKOV, A. N. & SHKADOV, V. YA. 1977 *Izv. Akad. Nauk SSSR Mekh. Zhid. i Gaza* **3**, 10.

KHADRA, L., KIM, Y. C., POWERS, E. J., JONES, F. L. & MIKSAD, R. W. 1981 *Computers in Flow Predictions and Fluid Dynamics Experiments* (ed. K. N. Ghia, T. J. Mueller & B. Patel). A.S.M.E. Book no. H 00201.

KIM, Y. C. & POWERS, E. J. 1978 *Phys. Fluids* **21**, 1452.

KIM, Y. C. & POWERS, E. J. 1979 *IEEE Trans. Plasma Sci.* PS-7, 120.

KIM, Y. C., KHADRA, L. & POWERS, E. J. 1980 *Phys. Fluids* **23**, 2250.

LASHINSKY, H. 1981 In *Proc. Symp. on Turbulence of Fluids and Plasmas*, p. 29. New York: Polytechnic Press.

MIKSAD, R. W., JONES, F. L. & POWERS, E. J. 1981 In *Proc. 7th Biennial Symp. on Turbulence, September* 1981, *Rolla, Missouri.*

MOLLO-CHRISTENSEN, E. & RAMANONJIARISOA, A. 1979 *J. Geophys. Res.* **84**, 7769.

MOTOHASHI, T. 1979 *Phys. Fluids* **22**, 1212.

PANTER, P. R. 1965 *Modulation, Noise, and Spectral Analysis.* McGraw-Hill.

SATO, H. 1970 *J. Fluid Mech.* **64**, 741.

SATO, H. & KURIKI, K. 1961 *J. Fluid Mech.* **11**, 321.

SATO, H. & SAITO, H. 1975 *J. Fluid Mech.* **67**, 539.

TARTER, M. E. & KRONMAL, R. A. 1967 *Proc. ACM* **22**, 511.